Title

Expression of Cationic Amino Acid Transporter 2 Is Required for Myeloid-Derived Suppressor Cell–Mediated Control of T Cell Immunity

Journal

The Journal of Immunology, 195(11)

ISSN

0022-1767

Authors

Cimen Bozkus, Cansu
Elzey, Bennett D
Crist, Scott A
et al.

Publication Date

2015-12-01

DOI

10.4049/jimmunol.1500959

Peer reviewed

The Journal of Immunology

Expression of Cationic Amino Acid Transporter 2 Is Required for Myeloid-Derived Suppressor Cell–Mediated Control of T Cell Immunity

Cansu Cimen Bozkus, Bennett D. Elzey, Scott A. Crist, Lesley G. Ellies and Timothy L. Ratliff

J Immunol 2015; 195:5237-5250; Prepublished online 21 October 2015;
doi: 10.4049/jimmunol.1500959
http://www.jimmunol.org/content/195/11/5237

The Journal of Immunology is published twice each month by
The American Association of Immunologists, Inc.,
1451 Rockville Pike, Suite 650, Rockville, MD 20852

Print ISSN: 0022-1767 Online ISSN: 1550-6606.

Expression of Cationic Amino Acid Transporter 2 Is Required for Myeloid-Derived Suppressor Cell–Mediated Control of T Cell Immunity

Cansu Cimen Bozkus,* Bennett D. Elzey,* Scott A. Crist,* Lesley G. Ellies,† and Timothy L. Ratliff*

Myeloid-derived suppressor cells (MDSCs) are a heterogeneous population of immature cells that expand during benign and cancer-associated inflammation and are characterized by their ability to inhibit T cell immunity. Increased metabolism of L-Arginine (L-Arg), through the enzymes arginase 1 and NO synthase 2 (NOS2), is well documented as a major MDSC suppressive mechanism. Therefore, we hypothesized that restricting MDSC uptake of L-Arg is a critical control point to modulate their suppressor activity. Using murine models of prostate-specific inflammation and cancer, we have identified the mechanisms by which extracellular L-Arg is transported into MDSCs. We have shown that MDSCs recruited to localized inflammation and tumor sites upregulate cationic amino acid transporter 2 (*Cat2*), coordinately with *Arg1* and *Nos2*. *Cat2* expression is not induced in MDSCs in peripheral organs. CAT2 contributes to the transport of L-Arg in MDSCs and is an important regulator of MDSC suppressive function. MDSCs that lack CAT2 have significantly reduced suppressive ability ex vivo and display impaired capacity for regulating T cell responses in vivo as evidenced by increased T cell expansion and decreased tumor growth in *Cat2*$^{-/-}$ mice. The abrogation of suppressive function is due to low intracellular L-Arg levels, which leads to the impaired ability of NOS2 to catalyze L-Arg–dependent metabolic processes. Together, these findings demonstrate that CAT2 modulates MDSC function. In the absence of CAT2, MDSCs display diminished capacity for controlling T cell immunity in prostate inflammation and cancer models, where the loss of CAT2 results in enhanced antitumor activity. ***The Journal of Immunology*****, 2015, 195: 5237–5250.**

Hematopoiesis is altered in inflammation and cancer. Such pathological conditions stimulate myelopoiesis, inhibit differentiation of immature myeloid cells, and induce their activation (1, 2). This heterogeneous population of immature myeloid cells, called myeloid-derived suppressor cells (MDSC), is important for controlling inflammation and, notably, have been shown to be recruited to benign and cancer-associated inflammation sites to block T cell immunity (1). MDSC-mediated suppression facilitates tumor progression and is associated with worse prognosis, increased metastatic tumor burden, and decreased survival of cancer patients (3, 4). Consequently, blockade of MDSC suppressor capacity has been suggested to be an essential component for improving antitumor immune responses (5). Therefore, MDSCs are a critical target for cancer immunotherapy. In addition, MDSCs have been shown to play beneficial roles in autoimmune diseases (6–8). Unfortunately, current strategies for controlling MDSC suppressor function have not found clinical application.

In mice, MDSCs are characterized by coexpression of CD11b and Gr-1 surface markers. MDSCs comprise heterogeneous mixtures of myeloid cells at early differentiation stages. The most recognized MDSC subpopulations are monocytic MDSC (M-MDSC) and granulocytic MDSC (G-MDSC) subsets, identified as $CD11b^{+}Ly6C^{high}Ly6G^{-}$ and $CD11b^{+}Ly6C^{low}Ly6G^{+}$, respectively (1). It is generally accepted that M-MDSCs are the dominant suppressor phenotype, but depending on the tumor model, G-MDSCs may mediate significant suppression as well (9, 10). MDSCs use multiple mechanisms to mediate T cell suppression. Increased expression and activities of arginase 1 (ARG1) and NO synthase 2 (NOS2) are well established as the hallmarks for MDSC suppressive function (11). Both enzymes use L-Arginine (L-Arg) as a common substrate and deplete L-Arg from the microenvironment, and produce NO, reactive oxygen species (ROS), and reactive nitrogen species, which mediate T cell suppression (11). Excessive ARG1 and NOS2 activities in MDSCs require L-Arg import (12). Despite its importance as the unique substrate for ARG1 and NOS2, the mechanism by which L-Arg is transported into MDSCs and the impact of L-Arg transport on suppressor function have not been defined.

There are four transporter systems for L-Arg uptake through mammalian cellular membranes: y^{+}, $y^{+}L$, $b^{o,+}$, $B^{o,+}$ (13). Among these systems, y^{+} shows higher selectivity for cationic amino acids, such as L-Arg, and is considered as the major route for L-Arg entry into cells (14). y^{+} system comprises four carrier proteins: CAT1–CAT4. The specific functions of CAT3 and CAT4 are

*Comparative Pathobiology Department, Purdue University Center for Cancer Research, Purdue University, West Lafayette, IN 47907; and †Department of Pathology, University of California, San Diego, La Jolla, CA 92093

Received for publication April 24, 2015. Accepted for publication September 24, 2015.

This work was supported by grants from the National Institute of Diabetes and Digestive and Kidney Diseases (Grant DK084454), the National Cancer Institute (Grant CA173918), and the Purdue Center of Cancer Research (Grants P30 CA023168 and K22CA118182).

Address correspondence and reprint requests to Dr. Timothy L. Ratliff, Comparative Pathobiology Department, Purdue University, 201 South University Street, Hansen Life Sciences Research Building, West Lafayette, IN 47907-2064. E-mail address: tlratliff@purdue.edu

The online version of this article contains supplemental material.

Abbreviations used in this article: ARG1, arginase 1; Cat2, cationic amino acid transporter 2; DCFDA, 2′,7′-dichlorofluorescin diacetate; G-MDSC, granulocytic MDSC; KO, Cat2 knockout mice; L-Arg, L-Arginine; L-Leu, L-leucine; L-NMMA, N^{G}-monomethyl-L-arginine; MDSC, myeloid-derived suppressor cell; M-MDSC, monocytic MDSC; NAC, *N*-acetyl-L-cysteine; NEM, *N*-ethyl maleimide; nor-NOHA, N^{ω}-hydroxy-L-arginine; NOS2, NO synthase 2; OTI, OVA-specific T cell; POET-3, prostate OVA-expressing mice-3; qPCR, quantitative PCR; ROS, reactive oxygen species; WT, wild type.

not well characterized. CAT1 is ubiquitously expressed, with the exception of adult liver. However, CAT1 transport of L-Arg is slow, and therefore cells with a high demand for L-Arg induce cationic amino acid transporter 2 (CAT2) expression to provide rapid transport of L-Arg to meet functional requirements (15). For example, activated macrophages upregulate CAT2 expression upon activation, and the lack of CAT2 results in a significant decrease in L-Arg transport and NO production, indicating CAT2 is required for sustained NOS2 activity (16, 17). Mature tumor-associated myeloid cells, $CD11b^{+}Gr\text{-}1^{-}$, also display increased CAT2 expression and the concomitant L-Arg uptake (18). Although CAT2 is well studied in the context of L-Arg transport in various cell types, its importance in transportation of L-Arg in MDSCs and its role as a regulator of MDSC suppressive function is unknown. Using murine models of prostate-specific inflammation and cancer, we investigated the role of CAT2 in MDSC suppressive activity. We provide evidence that *Cat2* is coordinately induced with *Arg1* and *Nos2*. The data show that CAT2 is an active transporter of L-Arg in MDSCs and its function is required for optimal suppressive activity. CAT2-deficient MDSCs display an impaired capacity for regulating T cell responses both ex vivo and in vivo.

Materials and Methods

Mice

C57BL/6 mice were purchased from Jackson Laboratories. $Cat2^{-/-}$ and prostate OVA-expressing mice-3 (POET-3) mice were generated as described previously (16, 19). $Cat2^{-/-}$POET-3 mice were generated by breeding $Cat2^{-/-}$ and POET-3 mice. $Rag^{-/-}Thy1.1^{+}$ OVA-specific T cell (OTI) mice were generated by breeding $Thy1.1^{+}$OTI mice and $Rag^{-/-}$ mice purchased from Jackson Laboratories. Both female and male mice between 7 and 12 wk of age were used for all tumor studies. For POET-3 experiments, only male mice were used. All animal experiments for this study were approved by the Purdue University Animal Care and Use Committee.

Animal models

C57BL/6 and $Cat2^{-/-}$ mice were used for tumor studies. For prostate cancer studies, 1×10^6 RM1 prostate cancer cells were injected i.p. Mice were sacrificed 6–7 d after tumor cell inoculation. For the bladder cancer model, 5×10^5 MB49 bladder cancer cells were injected s.c. in the flank area. Mice were sacrificed after 14 d when tumors reached 1.5 cm in diameter. For tumor growth experiments, mice were injected with 3×10^6 Fico/Lite (Atlanta Biologicals) purified EG7 or EL4 cells s.c. in the flank area or intradermally in the shoulder area. After 7 d, $1–1.5 \times 10^6$ activated OTIs were injected i.v. For the Winn assay, 3×10^6 EG7 or EL4 cells were injected intradermally in the shoulder area with or without 10^4 activated OTIs in the presence or absence of 10^4 $CAT2^{+/+}$ or $CAT2^{-/-}$ $CD11b^{+}Gr\text{-}1^{+}$ cells isolated from the ascites of RM1 mice. Tumor size was measured using calipers and calculated by the formula [(small diameter)^2 × (large diameter) × 0.5]. POET-3 and $Cat2^{-/-}$POET-3 mice were used for inflammation studies. Prostate inflammation was induced by i.v. injection of 5×10^6 in vitro–activated (48 h) OTIs into POET-3 mice. Mice were sacrificed 5 d after the induction of inflammation. For the adoptive transfer studies, 2 d after the induction of inflammation POET-3 mice received (i.p.) 4×10^6 MDSCs generated by culturing bone marrow cells with GM-CSF (40 ng/ml) and IL-6 (40 ng/ml) (purchased from Peprotech) for 5 d.

Cell isolation and generation

Bone marrow was collected from femurs and tibias. Spleens were harvested and ground using frosted slides. Cells from ascitic tumors were collected by flushing the peritoneal cavity with 10 ml PBS. Cells from solid tumors were collected by digesting the minced tissue at 37˚C for 1 h in media containing collagenase D (2 mg/ml; Roche Diagnostics) and DNAse I (10 μg/ml; Sigma-Aldrich). Cells from prostate glands were obtained by harvesting and pooling anterior, ventral, and dorsolateral lobes of prostates, and minced tissues were digested for an hour at 37˚C in media containing collagenase D (2 mg/ml). RBCs were lysed by using ACK buffer and cells were passed through a 70-μm filter. OTIs were isolated from the spleens of $Rag^{-/-}$OTI mice and activated by culturing in RPMI 1640 media containing SIINFEKL (1 μg/ml, Ova peptides 257–264, American peptide) and 2-ME (55 μM). Activated OTIs were purified by Fico/Lite. Macrophages were obtained by collecting cells from mice by washing the peritoneal cavity with 10 ml PBS 5 d after thioglycollate injection (i.p.). Cells were cultured and unattached cells were removed after 2 h. Macrophages were then cultured for another 17 h in the absence or presence of LPS (100 ng/ml; Sigma-Aldrich) and IFN-γ (25 ng/ml; Peprotech). For in vitro activation of MDSCs, $CD11b^{+}Gr\text{-}1^{+}$ cells were isolated from bone marrow by FACS and were cultured for 3 d with GM-CSF (40 ng/ml), IFN-γ (25 ng/ml), and IL-13 (33 ng/ml; Peprotech).

Flow cytometry

Single-cell suspensions were incubated with TruStain fcX (Clone 93) and stained with conjugated Abs. MDSCs were labeled with anti-CD11b (Clone M1/70), anti–Gr-1 (Clone RB6-8C5), anti–Ly-6C (Clone HK1.4), and anti–Ly-6G (Clone 1A8). T cells were labeled with anti-CD45 (Clone 30-F11), anti-CD8a (Clone 53-6.7), and anti-CD90.1 (Clone OX-7). To measure IFN-γ production by OTI, we cultured cells for 6–8 h in the presence of SIINFEKL and GolgiStop (BD Biosciences). After staining for surface Ags, cells were prepared for intracellular staining using the CytoFix/CytoPerm kit (BD Biosciences) and stained with anti–IFN-γ (Clone XMG1.2). Abs were purchased from BioLegend and used at 2 μg/ml concentration. OTI proliferation was measured using BrdU Flow Kit (BD Biosciences) or Click-iT EdU Flow Cytometry Assay Kit (Molecular Probes, Life Technologies) according to the manufacturer's instructions. For ARG1 and NOS2 protein detection, after surface Ag staining, cells were fixed and permeabilized using BD CytoFix/CytoPerm kit. Cells were then stained for ARG1 and NOS2 for 30 min at room temperature. ARG1 staining was performed in 20 μl of 25 μg/ml PE-conjugated anti-ARG1 polyclonal Ab or the isotype control PE-conjugated polyclonal sheep IgG (R&D Systems). For NOS2 detection, allophycocyanin-conjugated anti-NOS2 mAb (Clone CXNFT; eBioscience) and the allophycocyanin-conjugated mouse-IgG2a isotype control (Clone RMG2a-62) were used at 10 μg/ml. All analyses were performed using BD FACSCanto II, and data were analyzed using FlowJo software (Tree Star). All cell sorting was performed using a BD FACSAria III. Sort purities were >95%.

Quantitative real-time PCR

Total RNA was isolated from cells using the E.Z.N.A. Total RNA Kit I (Omega Bio-tek), and cDNA synthesis was performed using qScriptTM cDNA SuperMix (Quanta Biosciences) according to the manufacturer's instructions. Multiplex quantitative real-time PCR was performed using PerfeCTa FastMix II (Quanta Biosciences), PrimeTime quantitative PCR (qPCR) gene probes (IDT) including *Arg1* (Mm.PT.58.8651372), *Nos2* (Mm.PT.58.43705194), *Slc7a2* (Mm.PT.58.28825099), and endogenous control 18s rRNA (Applied Biosystems). Relative mRNA expression was calculated by the equation $2^{-[Ct(gene) - Ct(18s\ rRNA)]}$, where Ct is the threshold cycle value.

L-Arg transport assays

Isolated MDSCs were cultured overnight with GM-CSF (40 ng/ml), IFN-γ (25 ng/ml), and IL-13 (33 ng/ml). Peritoneal macrophages were cultured with LPS (100 ng/ml) and IFN-γ (25 ng/ml) for 17 h. Transport assays were carried out at 25˚C in a buffer containing 118.5 mM NaCl, 5.6 mM KCl, 1.3 mM $CaCl_2$, 0.6 mM $MgCl_2$, 11.1 mM glucose, 0.03 mM EDTA, 0.06 mM L-ascorbic acid, and 20 mM HEPES. Transport through the y^{+} system was blocked by pretreating cells with *N*-ethyl maleimide (NEM) (5 mM) (Sigma-Aldrich) at 25˚C for 5 min. To block transportation through the y^{+}L system, we added 5 mM L-Leucine (L-Leu) to the transport buffer. Cells were pulsed with L-[^{3}H]-Arginine (6 μCi/ml; PerkinElmer) for 3 min and were washed with stop solution (transport buffer containing 10 mM nonradioactive L-Arg). Cells were then lysed with 4% Triton X-100 and the uptake was measured using a scintillation counter. The protein concentration of cell lysates was measured using the Bradford assay (Sigma-Aldrich) according to the manufacturer's instructions. Uptake was represented as cpm/mg protein for normalization purposes.

MDSC functional assays

Sorted MDSCs or MDSC subsets were cocultured in 96-well U-bottom plates with OTIs (10^5 cells/well) preactivated for 8 h (or naive, where indicated) in media containing the cognate Ag SIINFEKL. OTI proliferation was measured by determining BrdU or EdU incorporation after 18 h for short-term assays and 48–72 h for long-term assays. BrdU and EdU were added 6 and 2 h before harvest, respectively. BrdU and EdU incorporation were measured by flow cytometry. Where indicated, N^G-monomethyl-L-arginine (L-NMMA; 0.5 mM; Calbiochem), N^{ω}-hydroxy-L-arginine (nor-NOHA; 0.5 mM; Calbiochem), and *N*-acetyl-L-cysteine (NAC;

1 or 10 mM; Sigma-Aldrich) were added to the suppression assay at the beginning of coculture. The percent suppression was calculated as [(1 − [proliferation with MDSCs]/[proliferation without MDSCs]) × 100]. IFN-γ production was measured by intracellular IFN-γ staining for flow cytometry.

Measurement of nitrite, ROS, and urea

Sorted cells were cultured for 24 h with or without LPS (100 ng/ml) and IFN-γ (25 ng/ml). Nitrite formation was quantified using the Standard Griess Assay (Molecular Probes, Life Technologies) according to the manufacturer's instructions. ROS formation was measured using 2′,7′-dichlorofluorescin diacetate (DCFDA)–Cellular ROS detection assay kit (Abcam) according to the manufacturer's instructions. In the arginase assay, sorted cells were lysed in 0.1% Triton X-100 containing protease inhibitors (Roche) at 10^7 cells/ml and incubated at room temperature for 30 min. Subsequently, equal volume of 10 mM $MnCl_2$ and 25 mM Tris-HCl (pH 7.5) were added. After 10-min incubation at 55˚C, equal volume of 0.5 M L-Arg (pH 9.7) was added. Five microliters of lysates was incubated for 2 h at 37˚C. BioAssay Systems Quantichrome Urea Assay Kit, which detects urea and citrulline equivalently (20), was used according to the manufacturer's instructions to determine arginase activity.

Statistical analysis

Data were presented as mean ± SEM. Statistical analyses were performed using GraphPad Prism software. The p values were calculated using Student t test and one-way ANOVA with Bonferroni's posttest when two or multiple groups were compared, respectively. Differences were considered significant when $p < 0.05$.

Results

Cat2 expression is induced in MDSCs upon acquisition of suppressive function

To assess whether *Cat2* expression is upregulated in MDSCs upon gaining suppressive activity, we used an in vitro system in which we isolated $CD11b^+Gr\text{-}1^+$ cells from bone marrow and cultured them with activating cytokines (IFN-γ, IL-13, and GM-CSF) for 3 d (21). After 3 d of culture with cytokines, MDSCs upregulated *Arg1* and *Nos2* expression and could suppress T cells (Figs. 1A, 1B). We compared *Cat2* expression levels in $CD11b^+Gr\text{-}1^+$ cells that were cultured with or without activating cytokines. We saw that *Cat2* expression was induced in activated MDSCs in parallel with *Arg1* and *Nos2* expression (Fig. 1C). To evaluate whether the induction of *Cat2* expression is coordinately regulated with *ArgI* and *Nos2* induction, we measured gene expression of in vitro–activated MDSCs after 24, 48, and 72 h of culture. The data show that the kinetics of *Cat2* induction in MDSCs parallels the induction of *ArgI* and *Nos2* expression (Fig. 1D). Next, we evaluated *Cat2* expression levels in $CD11b^+Gr\text{-}1^+$ cells isolated from tumor-bearing mice. We previously published that only MDSCs at the tumor site, but not at peripheral sites such as spleen, have immediate suppressive capacity (22). To investigate whether *Cat2* is indeed induced only in MDSCs with suppressive function, we compared *Cat2* expression in $CD11b^+Gr\text{-}1^+$ cells isolated from the spleen and tumor sites of tumor-bearing mice. To this end, we used a tumor model in which RM1 murine prostate cancer cells were injected i.p. into $Cat2^{+/+}$ mice (23). Six days after tumor inoculation, $CD11b^+Gr\text{-}1^+$ population was significantly expanded in the spleen and ascites of RM1-bearing mice compared with the naive control mice (Fig. 2A). $CD11b^+Gr\text{-}1^+$ cells were isolated from the spleen and ascites of RM1 i.p. tumor-bearing mice and from the spleen of naive mice. Only the MDSCs isolated from the tumor site, with immediate suppressive function, but not from spleens of naive or tumor-bearing mice had elevated *Cat2* expression (Fig. 2B). In addition, we examined *Cat2* expression in MDSC subsets (Fig. 2C). Both monocytic ($CD11b^+Ly6C^{high}Ly6G^-$) (M-MDSC) and granulocytic ($CD11b^+Ly6C^{low}Ly6G^+$) (G-MDSC) subsets at the tumor site displayed high *Cat2* expression unlike splenic counterparts (Fig. 2D). These data show that *Cat2* expression is induced in MDSCs with immediate suppressive function.

CAT2 regulates MDSC suppressive function

To evaluate whether CAT2 regulates MDSC suppressive function, we compared the suppressive ability of $Cat2^{+/+}$, $Cat2^{+/-}$, and $Cat2^{-/-}$ MDSC in vitro. After 3 d of culture with activating cytokines, bone marrow $CD11b^+Gr\text{-}1^+$ cells were cocultured with naive OTIs, OVA-specific $CD8^+$ T cells, in the presence of activating peptide. $Cat2^{-/-}$, but not $Cat2^{+/-}$, MDSCs displayed significantly reduced suppressive function compared with $Cat2^{+/+}$ MDSCs at all ratios (Fig. 3A). Because CAT2 needs to be completely absent to reduce suppressive capacity, for the rest of the study we used $Cat2^{+/+}$ (wild type [WT]) and $Cat2^{-/-}$ [Cat2 knockout mice (KO)] MDSCs. Next, we investigated whether $Cat2^{-/-}$ MDSCs isolated from tumor sites had lower suppressive function. We isolated $CD11b^+Gr\text{-}1^+$ cells from spleen and ascites of i.p. RM1 bearing WT and KO mice. Accumulation of $CD11b^+Gr\text{-}1^+$ cells at the tumor site, spleen, and bone marrow was comparable in both WT and KO animals (data not shown). To measure suppressive activity, we cultured isolated $CD11b^+Gr\text{-}1^+$ cells with preactivated OTIs for 18 h at differing ratios. This is a short-term assay and in this assay only MDSCs with immediate suppressor function are able to suppress OTI proliferation (22). As expected, precursor cells from spleen did not suppress OTI proliferation in 18 h, but WT MDSCs from tumor site were suppressive. Similar to in vitro–activated MDSCs, MDSCs isolated from tumor site possessed significantly reduced ability to suppress OTI proliferation in the absence of CAT2, where suppression by $CAT2^{-/-}$ MDSCs was observed only at a 2:1 MDSC/OTI ratio (Fig. 3B). Evaluation of the suppressive capacity of MDSCs in a long-term (48-h) suppression assay also demonstrated a similar reduced suppressive capacity of KO MDSCs (Fig. 3C). In addition, we determined intracellular IFN-γ levels of OTIs at the end of the culture. We observed that coculture with WT MDSCs resulted in fewer OTIs that displayed intracellular IFN-γ, further confirming the decreased suppressive capacity of CAT2-ablated MDSCs (Fig. 3D). To verify that our observations were not limited to the RM1 ascites model, we implanted mice with MB49 bladder cancer cells s.c. and monitored CAT2-dependent MDSC suppressive function in a 48-h culture (Supplemental Fig. 1A). MDSCs isolated from both tumor site and spleens of MB49 tumor-bearing animals had lower suppressive activity in the absence of CAT2, suggesting that our observations are broadly applicable. We also evaluated the suppressive capacity of MDSC subsets individually. Both M-MDSC and G-MDSC subsets displayed diminished suppressive capacity in the absence of CAT2 (Fig. 3E). In addition to tumor site MDSCs, we used MDSC subsets isolated from spleen and bone marrow. In a long-term assay, prolonged culture time enables MDSCs from peripheral sites to gain suppressive function because of exposure to endogenous and T cell–secreted activating factors. Therefore, unlike the results from short-term suppression assays, spleen and bone marrow MDSCs are expected to suppress T cells in a long-term assay (22). Accordingly, we observed that MDSCs from spleen and bone marrow displayed reduced suppressive action without CAT2 (Supplemental Fig. 1B). These results demonstrate that CAT2 is an important regulator of MDSC suppressive capacity. In the absence of CAT2, MDSCs display significantly reduced levels of suppressive activity.

CAT2 mediates L-Arg transportation in MDSCs

Because *Cat2* expression is elevated in parallel to L-Arg–dependent activities of *Arg1* and *Nos2* (12), we asked whether CAT2

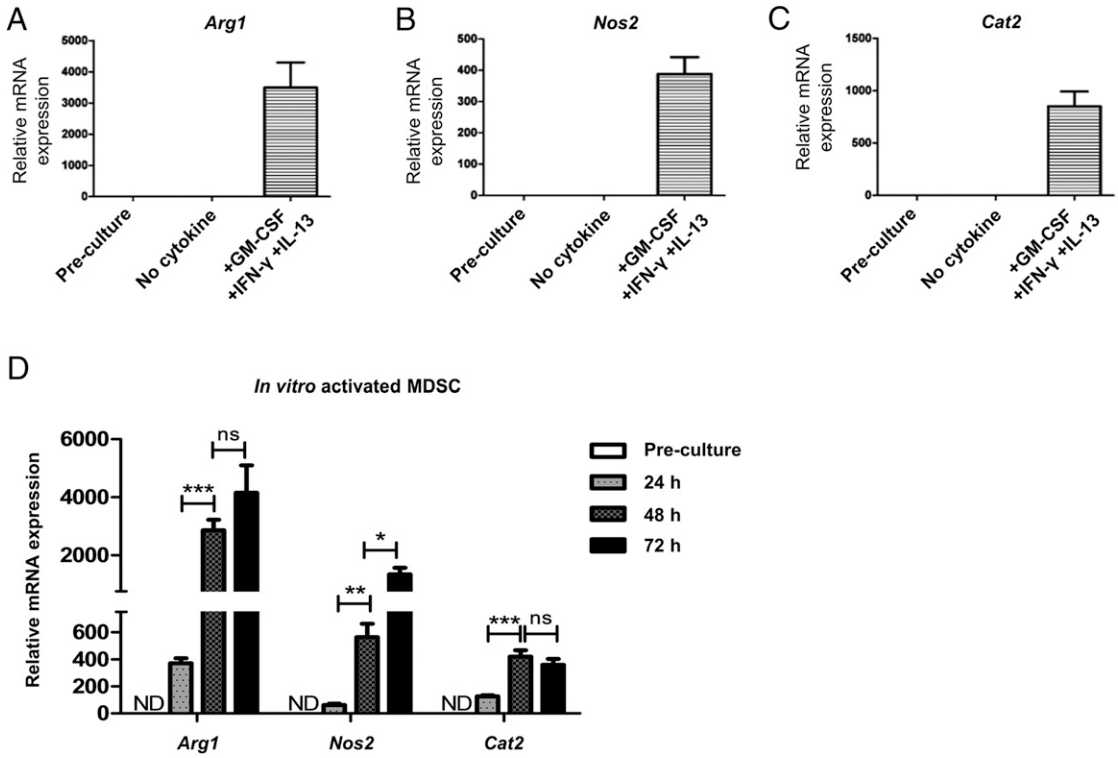

FIGURE 1. *Cat2* is coordinately induced with *Arg1* and *Nos2* in MDSCs. CD11b^{+}Gr-1^{+} cells were isolated from bone marrow of naive WT mice and cultured with or without GM-CSF, IL-13, and IFN-γ. mRNA was isolated after 3 d of culture (**A**) or every 24 h during culture ($n = 4$ mice, $^{**}p = 0.0027$, $^{*}p = 0.0211$, $^{***}p < 0.001$) (**B**). *Arg1*, *Nos2*, and *Cat2* gene expression were analyzed by qPCR. Data are representative of at least three independent experiments. For all experiments, errors bars indicate ± SEM.

was modulating L-Arg intake in MDSCs. To measure L-Arg intake, we used MDSCs isolated from ascites of i.p. RM1 bearing WT and KO mice. It has been reported that CAT2 plays a crucial role in L-Arg transport of activated thioglycollate-elicited peritoneal macrophages (16). Therefore, we used macrophages from WT and KO mice as a control. We measured L-[^{3}H]-Arginine uptake in activated macrophages (Fig. 4A) and tumor site MDSCs (Fig. 4B). As reported (16), in activated macrophages when CAT2 was absent, the reduction in L-Arg uptake was ~90%. As we anticipated, in MDSCs, L-Arg uptake was significantly lower in the absence of CAT2. Interestingly, in MDSCs, L-Arg transport was much lower than macrophages when standardized to protein levels, and CAT2-mediated L-Arg transport corresponded to only ~20% of total transport. Even so, CAT2-mediated transport is essential for optimal suppressive activity. There are multiple transportation systems that carry extracellular L-Arg into the cell. To eliminate the possibility that in KO MDSCs an alternate transporter is overexpressed and is compensating for the lack of CAT2, we investigated the expression levels of all members of L-Arg transporter systems in WT and KO MDSCs by qPCR (Supplemental Fig. 2). Data show that none of the amino acid transporters that can transport L-Arg are overexpressed in KO MDSCs. In addition, data revealed that in MDSCs, only the members of y^{+} and $y^{+}L$ systems are expressed. We could not detect any expression of transporters that are members of $b^{0,+}$ and $B^{0,+}$ systems. Next, we evaluated the specific contribution of y^{+} and $y^{+}L$ systems in L-Arg uptake in MDSCs. To this end, we used an inhibitor, NEM, that can block L-Arg transportation through the y^{+} system. NEM treatment blocked ~25% of total transport in intact MDSCs. Importantly, the inhibition of L-Arg transport in intact MDSCs upon the blockade of y^{+} system was comparable with the inhibition in CAT2$^{-/-}$ MDSCs, indicating that CAT2 is the major y^{+} system transporter in MDSCs. Accordingly, the total L-Arg transportation through CAT1, CAT3, and CAT4 was significantly lower than L-Arg uptake through CAT2 (Fig. 4C). To determine the contribution of $y^{+}L$ system, we measured L-Arg uptake in the presence or absence of 5 mM L-Leu. Addition of excessive amounts of L-Leu to the transportation medium competitively blocks L-Arg transportation through the $y^{+}L$ system. Data showed that the $y^{+}L$ system carries out ~25% of the L-Arg uptake in MDSCs and in accordance with the gene expression data, both WT and KO MDSCs had similar $y^{+}L$ system activities (Fig. 4D). Together, these results show that CAT2 is an important carrier of L-Arg in MDSCs, yet it is not the only transporter that mediates L-Arg uptake.

Lower suppressive capacity of CAT2$^{-/-}$ MDSCs is due to reduced NO production

Next, we evaluated the mechanisms through which CAT2 modulates MDSC suppressor function. One of the major suppressive mechanisms in MDSCs is the production of NO by NOS2. Because NOS2 uses L-Arg as its substrate to produce NO and CAT2 ablated MDSCs have lower L-Arg uptake, we hypothesized that CAT2 KO MDSCs have reduced NO production. To test this, we measured nitrite production in WT and KO MDSCs and MDSC subsets using a standard Griess reaction (Fig. 5A, 5B). We used activated macrophages as a control, because it is reported that, in the absence of CAT2, activated macrophages have a 92% reduction in NO production (16) (Fig. 5C). As expected, WT MDSCs produced significantly higher levels of NO. To eliminate the possibility that reduced NO formation in CAT2$^{-/-}$ MDSCs could be caused by diminished NOS2 expression in the absence of CAT2, we inspected NOS2 protein levels in CAT2$^{+/+}$ and CAT2$^{-/-}$ MDSC subsets. Data showed that NOS2 expression was similar in CAT2$^{+/+}$

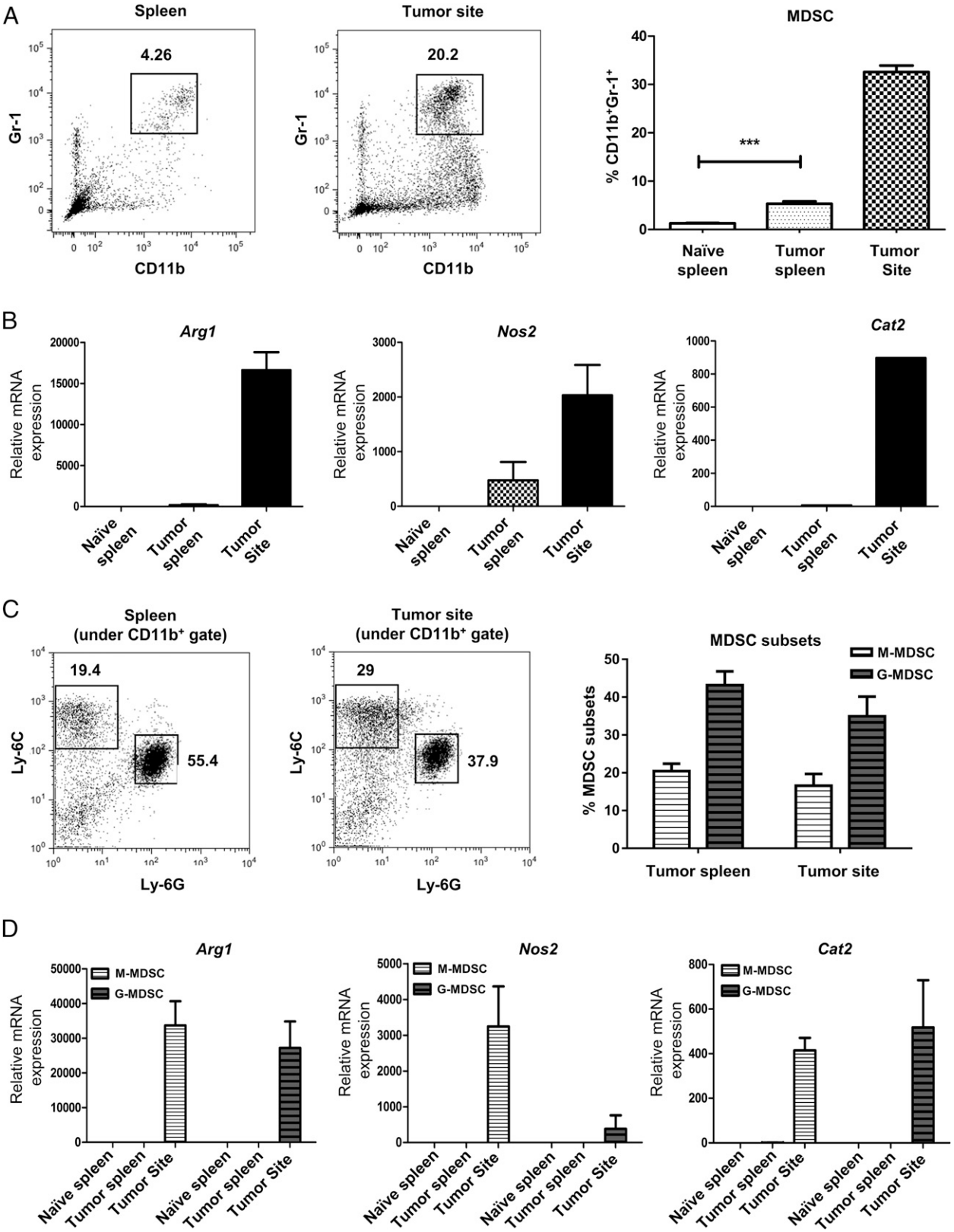

FIGURE 2. *Cat2* is induced in functionally active MDSCs. $CD11b^+Gr\text{-}1^+$ and $CD11b^+Ly6C^{high}Ly6G^-$ (M-MDSC), $CD11b^+Ly6C^{low}Ly6G^+$ (G-MDSC) cells were isolated by FACS from ascites and spleen of RM1 i.p. tumor-bearing $Cat2^{+/+}$ (WT) mice 6 d after tumor implantation or from the spleens of naive mice. The percentage of $CD11b^+Gr\text{-}1^+$ cells were demonstrated under side scatter/forward scatter gate ($n = 4$, $^{***}p = 0.0002$) (**A**). Percentages of $CD11b^+Ly6C^{high}Ly6G^-$ (M-MDSC) and $CD11b^+Ly6C^{low}Ly6G^+$ (G-MDSC) were demonstrated under $CD11b^+$ gate. Data are pooled from six independent experiments (**C**). mRNA was freshly isolated and analyzed by qPCR for *Arg1*, *Nos2*, and *Cat2* expression (**B** and **D**). Data are representative of at least three independent experiments. For all experiments, errors bars indicate ± SEM.

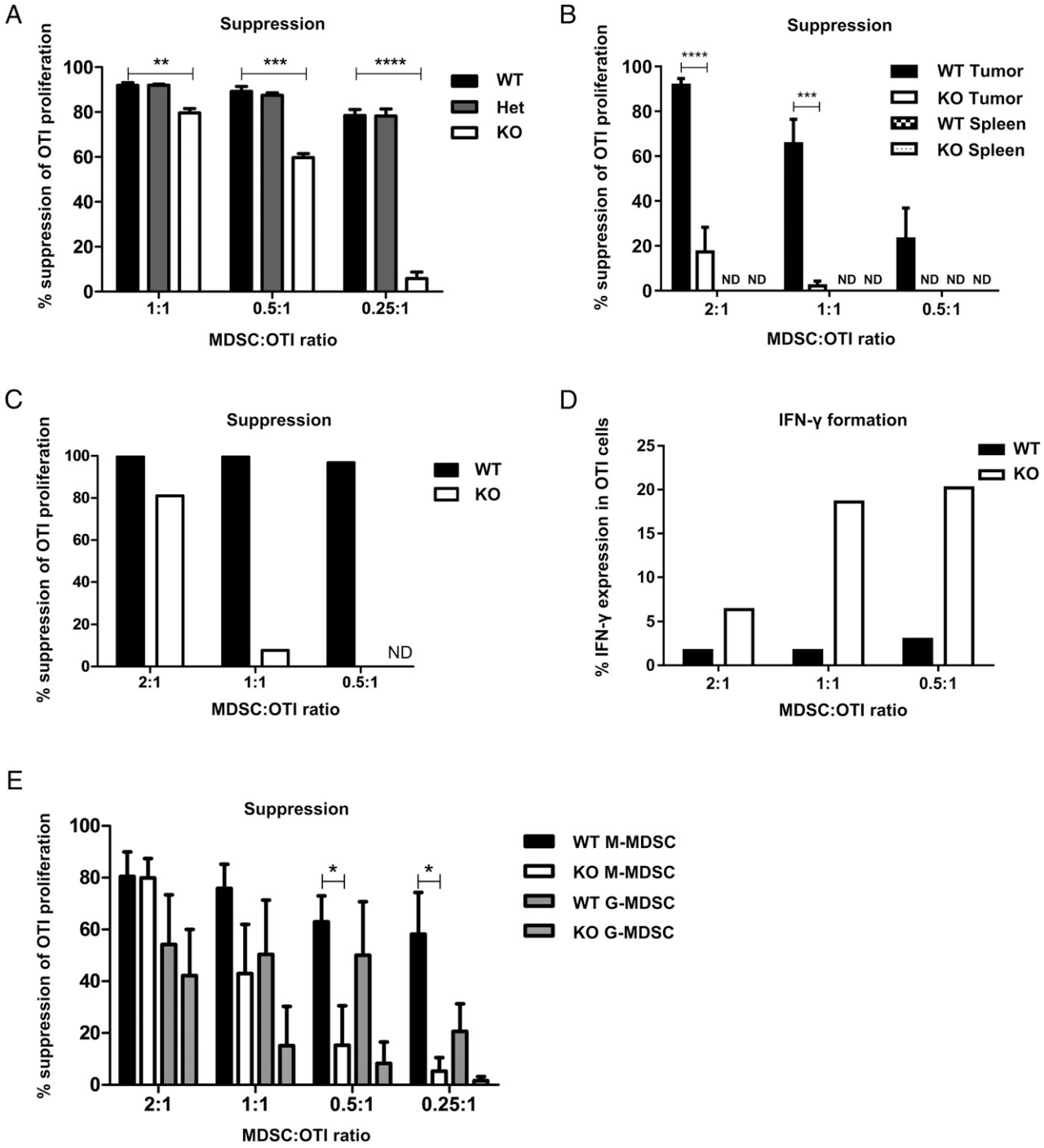

FIGURE 3. MDSC suppressive capacity is reduced in the absence of CAT2. $CD11b^{+}Gr\text{-}1^{+}$ cells were isolated from bone marrow of naive mice and cultured with GM-CSF, IL-13, and IFN-γ. After 3 d, cells were harvested and cocultured with naive OTI in the presence of SIINFEKL at indicated ratios for another 3 d. BrdU was added 6 h before harvest. OTI proliferation was evaluated by measuring BrdU incorporation. Data are representative of three independent experiments (n = 3–4/group, $^{**}p = 0.0057$, $^{***}p = 0.0001$, $^{****}p < 0.0001$) (**A**). $CD11b^{+}Gr\text{-}1^{+}$ cells were isolated from tumor site and spleens of RM1 bearing WT and KO mice (n = 3–5/group, pooled) 6 d after tumor implantation and cocultured with preactivated OTIs for 18 h. BrdU was added 6 h before harvest. OTI proliferation was evaluated by measuring BrdU incorporation. Data are pooled from three and five independent experiments for tumor and for spleen, respectively ($^{***}p = 0.0002$, $^{****}p < 0.0001$) (**B**). $CD11b^{+}Gr\text{-}1^{+}$ cells from the ascites of RM1 i.p. tumor-bearing $Cat2^{+/+}$ (WT) and $Cat2^{-/-}$ (KO) mice (n = 5/group, pooled) were cocultured with naive OTI cells with SIINFEKL for 48 h. BrdU and protein transport inhibitor were added 6 h before harvest. OTI proliferation was evaluated by measuring BrdU incorporation (**C**). IFN-γ levels in OT-I cells were determined by flow cytometry for intracellular IFN-γ staining (**D**). Data are representative of five independent experiments. M-MDSCs and G-MDSCs were isolated by FACS from the ascites of RM1 i.p. tumor-bearing WT and KO mice (n = 3–5/group, pooled) 6 d after tumor implantation and cocultured with naive OTI cells with SIINFEKL for 48–72 h. BrdU was added 6 h before harvest. OTI proliferation was evaluated by measuring BrdU incorporation. Data are pooled from five independent experiments ($^{*}p = 0.0312$ at 0.5:1 and $^{*}p = 0.0139$ at 0.25:1) (**E**). For all experiments, errors bars indicate ± SEM.

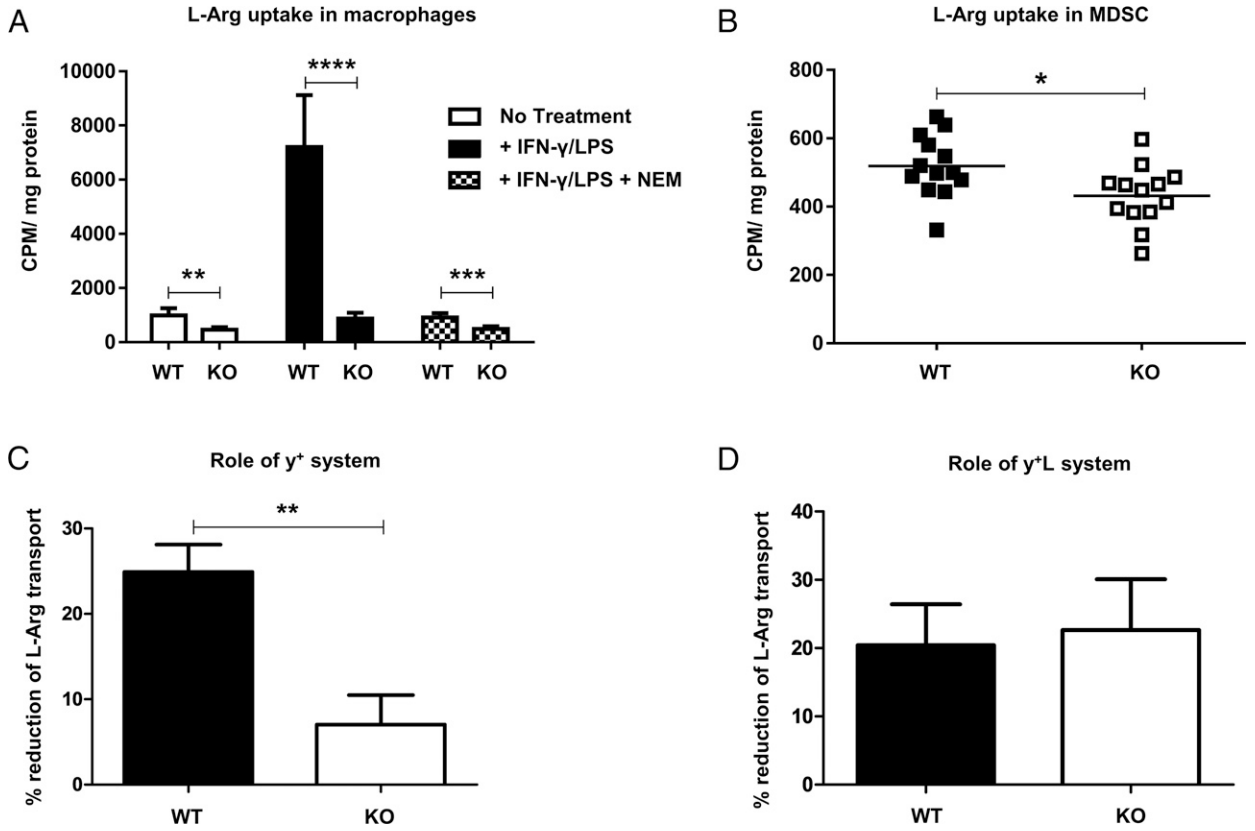

FIGURE 4. CAT2 mediates L-Arg transportation in MDSCs. Thioglycollate-elicited peritoneal macrophages from *Cat2*$^{+/+}$ (WT) and *Cat2*$^{-/-}$ (KO) mice (n = 5/group) were activated with LPS and IFN-γ for 18 h. L-Arg transport was measured by using 6 μCi/ml L-[^{3}H]-Arg in Na^+-containing buffer. For NEM, cells were pretreated with 5 mM NEM for 5 min and washed with transport buffer before measuring uptake. Data are representative of three independent experiments. $^{**}p = 0.0032$, $^{***}p = 0.0009$, $^{****}p < 0.0001$ (**A**). $CD11b^+Gr\text{-}1^+$ cells were isolated from ascites of RM1 tumor-bearing WT and KO mice and cultured overnight with GM-CSF, IL-13, and IFN-γ. Total L-Arg transport was measured by using 6 μCi/ml L-[^{3}H]-Arg in Na^+-containing buffer. Data are pooled from three independent experiments. n = 13/group, $^*p = 0.0184$ (**B**). Data correspond to reduction of total L-[^{3}H]-Arg transport when y^+ system was blocked using 5 mM NEM in WT and KO MDSCs. Data are pooled from three independent experiments (n = 10/group, $^{**}p = 0.0016$) (**C**). Data correspond to reduction of total L-[^{3}H]-Arg transport when y^+L system was blocked because of the presence of 5 mM L-Leu in transport media. Data are pooled from four independent experiments (n = 13/group) (**D**). All error bars indicate ± SEM.

and $CAT2^{-/-}$ MDSCs. Notably, in agreement with gene expression data (Fig. 2D), NOS2 protein expression was also mostly confined to the M-MDSC subset (Fig. 5D). Freshly isolated MDSCs from $CAT2^{+/+}$ and $CAT2^{-/-}$ also were tested for NOS2 levels, and although lower levels were present, the levels were comparable between the two phenotypes (Supplemental Fig. 3). Together, these data indicate that NOS2 expression in MDSCs is not modulated by CAT2 and hence the reduced NO formation in $CAT2^{-/-}$ MDSCs is likely to be due to diminished L-Arg uptake.

Another important suppressive mechanism MDSCs use for inhibiting T cell responses is the activity of ARG1 (11). CAT2 has been reported to modulate ARG1 activity in macrophages (24). Therefore, we investigated the possibility that CAT2 might be modulating ARG1 activity in MDSCs. ARG1 catalyzes L-Arg to L-Ornithine and urea (11). Thus, we measured urea formation in $CAT2^{+/+}$ and $CAT2^{-/-}$ MDSCs to inspect the role of CAT2 in ARG1 activity. As expected, tumor MDSCs had much greater ARG1 activity than bone marrow $CD11b^+Gr\text{-}1^+$ cells. Importantly, the data demonstrate that ARG1 activity is comparable in $CAT2^{+/+}$ and $CAT2^{-/-}$ MDSCs (Fig. 5E). Next, we measured ARG1 protein levels in $CAT2^{+/+}$ and $CAT2^{-/-}$ tumor MDSCs. In agreement with urea production observed, where L-Arg is supplied as a biochemical measure of relative ARG1 activity, we detected similar ARG1 protein levels in $CAT2^{+/+}$ and $CAT2^{-/-}$ MDSCs (Fig. 5F).

To evaluate the contribution of NOS2 and ARG1 to MDSC suppressive function, we used NOS inhibitor, L-NMMA, and arginase inhibitor, nor-NOHA. L-NMMA completely inhibited MDSC suppressive function. However, nor-NOHA had no effect on MDSC suppressive function (Fig. 5G). Thus, the data suggest that NOS2 metabolism is the major suppressive mechanism in MDSCs from the RM1 ascites tumor model. These data suggest that the reduced NO production in $CAT2^{-/-}$ MDSCs accounts for the reduced suppressive capacity.

Elevated ROS production in $CAT2^{-/-}$ MDSCs contributes to the suppressor activity

Although reduced, high levels of MDSCs still possess suppressive ability in the absence of CAT2. Hence we aimed to determine the mechanisms that regulate MDSC suppressive activity in a CAT2-independent manner. Previously, L-Arg availability has been shown to modify NOS2 function such that when L-Arg is depleted in the local environment, NOS2 produces mostly $\cdot O_2^-$ instead of NO (25). $\cdot O_2^-$ can react with other molecules, such as H_2O and NO, and produce ROS, thereby suppressing T cells (26). Therefore, we asked whether KO MDSCs had higher levels of ROS production. We measured ROS levels in WT and KO MDSCs by DCFDA staining and found that KO MDSCs had significantly higher ROS levels compared with WT MDSCs (Fig. 6A). DCFDA staining of MDSC subsets revealed that ROS production in M-MDSCs was similar in the absence or presence of CAT2, and the differential ROS production could be attributed to G-MDSCs (Fig. 6B).

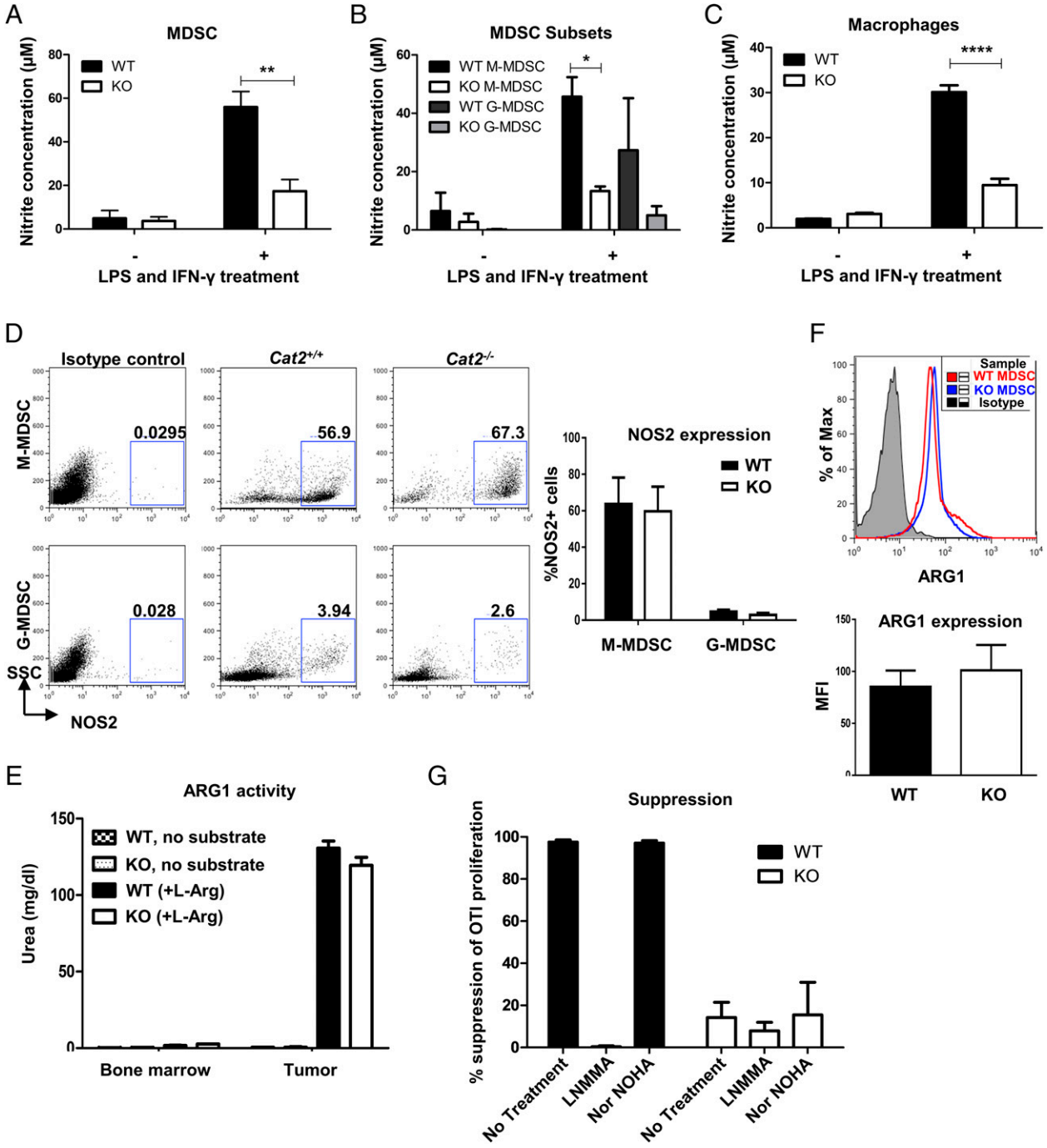

FIGURE 5. *Cat2*$^{-/-}$ MDSCs have reduced NO production. CD11b^{+}Gr-1^{+} MDSCs (**A**) and CD11b^{+}LyC^{high}Ly6G^{-} (M-MDSC) and CD11b^{+}LyC^{low} Ly6G^{+} (G-MDSC) subsets (**B**) were isolated from tumor site of RM1 bearing *Cat2*$^{+/+}$ (WT) and *Cat2*$^{-/-}$ (KO) mice. Cells were cultured in the presence and absence of LPS and IFN-γ for 24 h. Nitrite formation upon stimulation with LPS and IFN-γ was measured in a Griess Assay. Data are pooled from two independent experiments (n = 5–9 mice/group for MDSC, $^{**}p = 0.0065$; n = 4/group, pooled for subsets, $^{*}p = 0.0426$). Thioglycollate-elicited peritoneal macrophages from *Cat2*$^{+/+}$ (WT) and *Cat2*$^{-/-}$ (KO) mice (n = 4/group) were activated with LPS and IFN-γ for 18 h. Nitrite formation was measured in a Griess Assay. Data are representative of at least two independent experiments ($^{****}p < 0.0001$) (**C**). Cells from the ascites of WT and KO RM1 mice were cultured with LPS and IFN-γ overnight before intracellular staining of NOS2 for flow cytometry. Percentages of NOS2^{+} cells were demonstrated under CD11b^{+}LyC^{high}Ly6G^{-} (M-MDSC) and CD11b^{+}LyC^{low}Ly6G^{+} (G-MDSC) gates (n = 4–5/group). Data are representative of three independently performed experiments (**D**). Quantichrome Urea Assay Kit that measures urea and citrulline was used to measure arginase activity in CD11b^{+}Gr-1^{+} cells freshly isolated from the bone marrow and ascites of WT and KO RM1 mice (n = 4/group) with or without supplementing L-Arg. Data are representative of three independent experiments (**E**). Cells freshly isolated from the ascites of WT and KO RM1 mice were stained with anti-ARG1 Ab. ARG1 expression was detected by flow cytometry. Mean fluorescent intensity (MFI) of ARG1 expression was reported under CD11b^{+}Gr-1^{+} gate (n = 4/group). Data are representative of three independently performed experiments (**F**). WT and KO MDSCs were used in a 48-h suppression assay at 2:1 (MDSC/OTI) ratio in the presence or absence of NOS inhibitor, L-NMMA (0.5 mM), or ARG inhibitor, nor-NOHA (0.5 mM). BrdU was added 6 h before harvest. OTI proliferation was evaluated by measuring BrdU incorporation. Data were pooled from three independent experiments (**G**). For all experiments, errors bars indicate ± SEM.

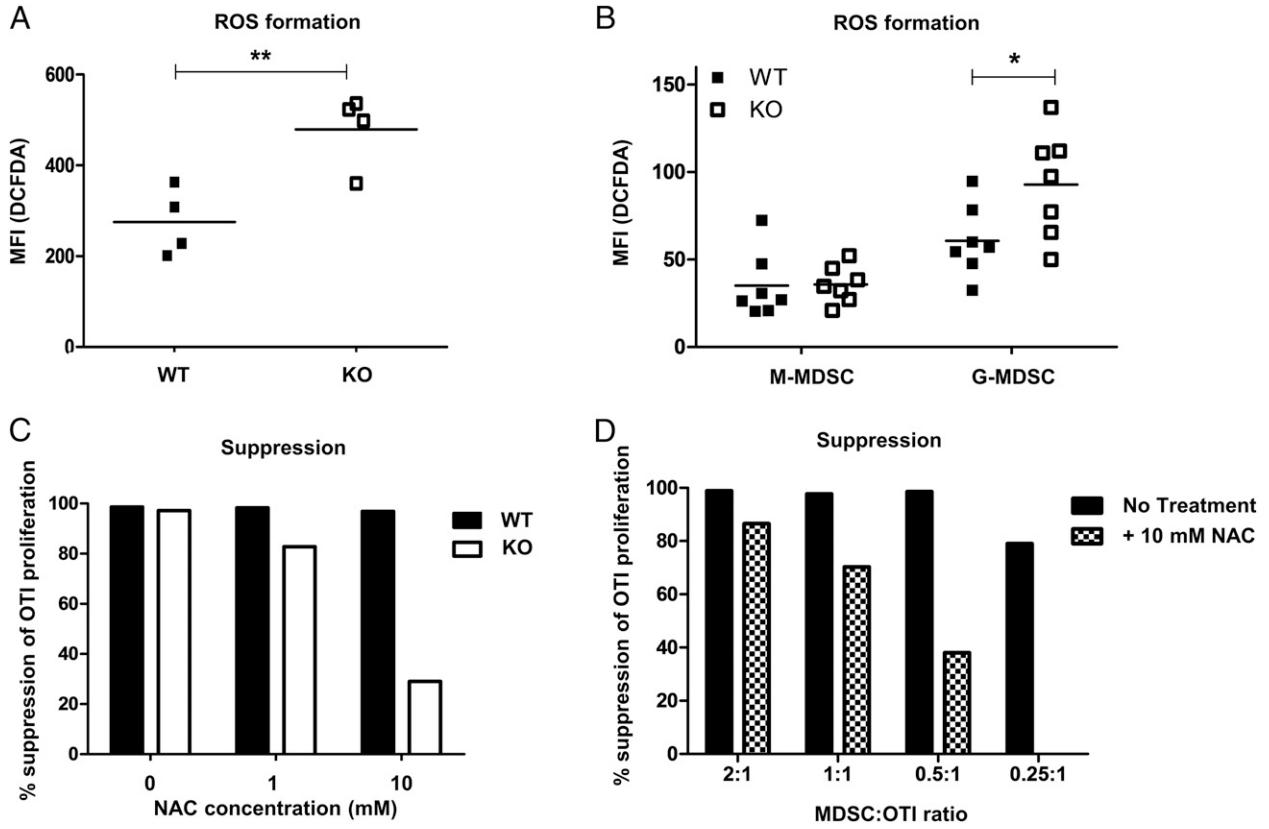

FIGURE 6. *Cat2*$^{-/-}$ MDSCs have increased ROS formation. Cells from ascites of i.p. RM1 bearing WT and KO mice were analyzed for ROS levels. DCFDA signal was analyzed under the gates for CD11b^{+}Gr-1^{+} (n = 4/group, $^{**}p$ = 0.0099) (**A**) and CD11b^{+}LyC^{high}Ly6G^{-} (M-MDSC) and CD11b^{+}LyC^{low} Ly6G^{+} (G-MDSC) subsets (n = 7/group, $^{*}p$ = 0.0376, data are pooled from two independent experiments) (**B**). Signal intensity was represented as mean fluorescent intensity (MFI). CD11b^{+}Gr-1^{+} cells were isolated by FACS from the ascites of RM1 i.p. tumor-bearing *Cat2*$^{+/+}$ (WT) and *Cat2*$^{-/-}$ (KO) mice (n = 5/group, pooled) 6 d after tumor implantation, and suppression assay was performed at 2:1 (MDSC/OTI) ratio in the presence of differing concentrations of ROS inhibitor, NAC (**C**). WT MDSCs were used for suppression assay at indicated MDSC/OTI ratios with or without 10 mM NAC (**D**). Data are representative of at least two independent experiments. All suppression assays were performed by coculturing MDSCs with preactivated OTI cells for 48 h. BrdU was added 6 h before harvest. OTI proliferation was evaluated by measuring BrdU incorporation. For all experiments, errors bars indicate ± SEM.

Next, we investigated the role of ROS formation in regulating MDSC suppressive function. We hypothesized that because of enhanced levels of production, in KO MDSCs, ROS plays a greater role in suppressive activity compared with WT MDSCs. To this end, we used ROS inhibitor NAC to assess the role of ROS in the suppressive function. Because CAT2$^{-/-}$ MDSCs have low inhibitory activity, we used a high MDSC/OTI ratio (2:1) in the suppression assay to capture the expected reductions in suppressor activity caused by the inhibition of ROS. As expected, NAC greatly reduced the suppressive capacity of KO MDSCs; however, it had no effect on WT MDSCs (Fig. 6C). Because ROS were previously shown to mediate the suppressive function of MDSCs (26), we concluded that the reason NAC did not affect suppressive activity of WT MDSCs was due to the high MDSC/OTI ratio in the suppression assay. To address this, we cocultured WT MDSCs at differing ratios with OTIs and determined the suppressive activity in the absence or presence of NAC. The results showed that at lower MDSC/OTI ratios ROS contributes to the suppressive activity of WT MDSCs (Fig. 6D). Together, these data suggest that ROS production can mediate MDSC suppressive activity in a CAT2-independent manner, and its role is enhanced in KO MDSCs because of the elevated levels.

CAT2$^{-/-}$ *MDSCs display diminished capacity for controlling T cell immunity in vivo*

To evaluate whether CAT2 can modulate MDSC regulatory functions in vivo, we performed a Winn assay, in which 3 × 10^{6} EG7 lymphoma cells were injected intradermally with or without activated OTI cells (27) in the presence or absence of MDSCs. EG7 express OVA and hence are susceptible to killing by OTI cells. EG7 tumors when implanted alone grew progressively. The presence of 10^{4} OTIs was sufficient to block tumor growth. In the presence of WT MDSCs, OTI cells did not significantly inhibit tumor growth and, although slower, tumors grew progressively (Fig. 7A). To the contrary, the presence KO MDSCs had no effect on OTI function (Fig. 7A). We further analyzed the role of CAT2 in vivo using another tumor model that allowed us to investigate CAT2-mediated effects on the regulatory function of endogenous tumor-induced MDSCs. We implanted 3 × 10^{6} EG7 lymphoma cells intradermally into WT and KO mice. Seven days after injection, we adoptively transferred 1 × 10^{6} activated OTIs i.v. and monitored tumor growth. Tumor growth was slower in KO mice (Fig. 7B). Accordingly, we observed significantly slower tumor progression in KO mice when EG7 tumors were implanted s.c. (Supplemental Fig. 4). Together, these observations suggest that the ability of MDSCs to regulate effector T cell function in vivo is impaired in the absence of CAT2.

Absence of CAT2 decreases the regulatory function of MDSCs in an acute inflammation model

CAT2 is important in regulating MDSC function in a tumor-induced setting of chronic inflammation. To expand these findings to MDSCs found in acute inflammatory sites, we used a

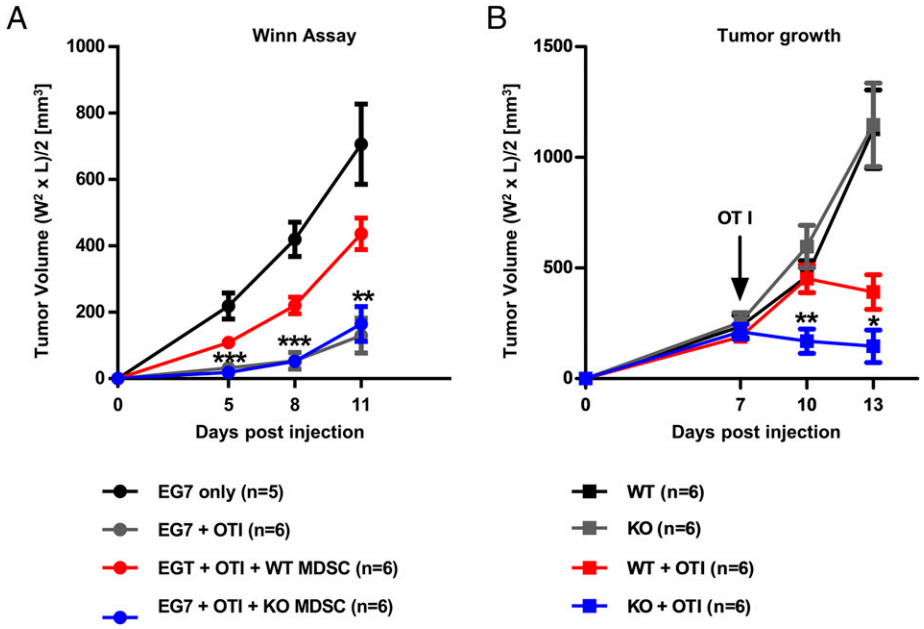

FIGURE 7. CAT2$^{-/-}$ MDSCs display diminished capacity for controlling T cell immunity in vivo. *Cat2*$^{-/-}$ mice were injected intradermally with 3×10^6 EG7 lymphoma cells alone, 3×10^6 EG7 with 10^4 activated OTIs, 3×10^6 EG7 with 10^4 activated OTIs, and 10^4 *Cat2*$^{+/+}$ or *Cat2*$^{-/-}$ CD11b$^+$Gr-1$^+$ cells. Data are pooled from two independent experiments (n = 5–6 mice/group). The p values for the comparison of WT or KO MDSC received groups are 0.0001, 0.0003, and 0.0033 on days 5, 8, and 11, respectively (**A**). *Cat2*$^{+/+}$ and *Cat2*$^{-/-}$ mice were injected intradermally with 3×10^6 EG7 lymphoma cells. Seven days after tumor inoculation, mice were i.v. injected with 10^6 activated OTI cells (n = 6/group). Tumor growth was monitored. The p values for the comparison of WT and KO mice that received OTIs are 0.0072 and 0.0449 on days 10 and 13, respectively (**B**). Tumor size was calculated as $(W^2 \times L)/2$ [mm^3]. Errors bars indicate ± SEM.

prostate-specific inflammation model, POET-3 (28). POET-3 express the chicken egg OVA gene under the control of the prostate-specific probasin promoter. Hence adoptive transfer of OTIs results in induction of prostate-specific inflammation (28) with MDSC recruitment to prostate and spleen (Fig. 8A). MDSCs isolated from prostate, but not from spleen, can suppress T cell responses (22). We isolated CD11b$^+$Gr-1$^+$ cells from prostate and spleens of inflamed POET-3 mice and investigated *Cat2* expression levels. Similar to the results we obtained from the RM1 tumor model, *Cat2* is coordinately upregulated with *Arg1* and *Nos2* in only MDSCs isolated from prostate (Fig. 8B). To evaluate the role of CAT2 in MDSCs in an acute inflammatory model, we bred our POET-3 mice with CAT2$^{-/-}$ mice. We investigated MDSC accumulation in CAT2 WT and KO POET-3 mice. Accumulation of both MDSC and MDSC subsets from the prostate and spleen were comparable between WT and KO POET-3 mice (data not shown). Next, we evaluated whether CAT2 modulated the suppressive capacity of MDSCs. As seen in the tumor models, MDSCs from acute inflammatory sites also had reduced suppressive capacity in the absence of CAT2 (Fig. 8C). Furthermore, we investigated whether CAT2 was modulating MDSC regulatory function in vivo. Because the absence of CAT2 results in reduced MDSC function, we hypothesized that in KO POET-3 mice the ability of MDSCs to inhibit T cells should be diminished, leading to a greater OTI population in the prostate. OTI cells express Thy1.1 and, using this congenic marker, we can monitor adoptively transferred OTI cells. We investigated the OTI population in prostate and spleens of WT and KO POET-3 mice. As expected, the KO POET-3 prostate had significantly more OTI cells, both as population percentages and absolute numbers (data not shown). To ensure that the increase in OTI cells in the KO POET-3 prostate was due to MDSC activity, we adoptively transferred WT MDSCs into KO POET-3 mice. It was previously shown that culturing bone marrow cells with GM-CSF and IL-6 expand the CD11b$^+$Gr-1$^+$ population (9, 29). We isolated bone marrow from naive WT and KO mice and cultured the cells for 5 d with GM-CSF and IL-6. Then we transferred these in vitro–generated KO MDSCs into KO POET-3 and WT MDSCs into WT or KO POET-3. As expected, the OTI population in the KO POET-3 was significantly greater than in WT POET-3 prostates. Adoptive transfer of WT MDSCs into KO POET-3 could partially rescue this phenotype (Fig. 8D). Only MDSCs in the prostate, but not the spleen, have suppressive function; therefore, MDSCs in the spleen should not regulate OTI cells. As expected, WT and KO POET-3 have comparable OTI numbers in the spleens (Fig. 8E). In addition, we investigated IFN-γ formation in OTI cells from WT and KO POET-3. OTIs isolated from the prostates of KO POET-3 trend toward higher levels of IFN-γ (Fig. 8F). OTIs from the spleen displayed similar IFN-γ levels in WT and KO POET-3 mice (Fig. 8G).

In summary, these data suggest that elevated CAT2 expression is a marker of MDSCs that acquired suppressive function, unlike those in spleen or bone marrow. CAT2 regulates MDSC suppressive capacity and is important for MDSCs to have complete regulatory control of T cell immunity.

Discussion

MDSCs are one of the dominant immunosuppressive populations that are present in the tumor microenvironment, impairing T cell function and promoting tumor progression (30). Therefore, MDSCs present a major obstacle for the success of cancer immunotherapy. As a result, blocking MDSC function has been an attractive endeavor to complement cancer therapies. Indeed, several studies demonstrated that depletion of MDSCs or inhibiting MDSC function impaired cancer progression (31, 32). Although these studies are very promising, more specific strategies to block MDSC suppressive function are needed.

MDSCs mediate their inhibitory effects on T cells through diverse mechanisms (33). One mechanism is the metabolism of

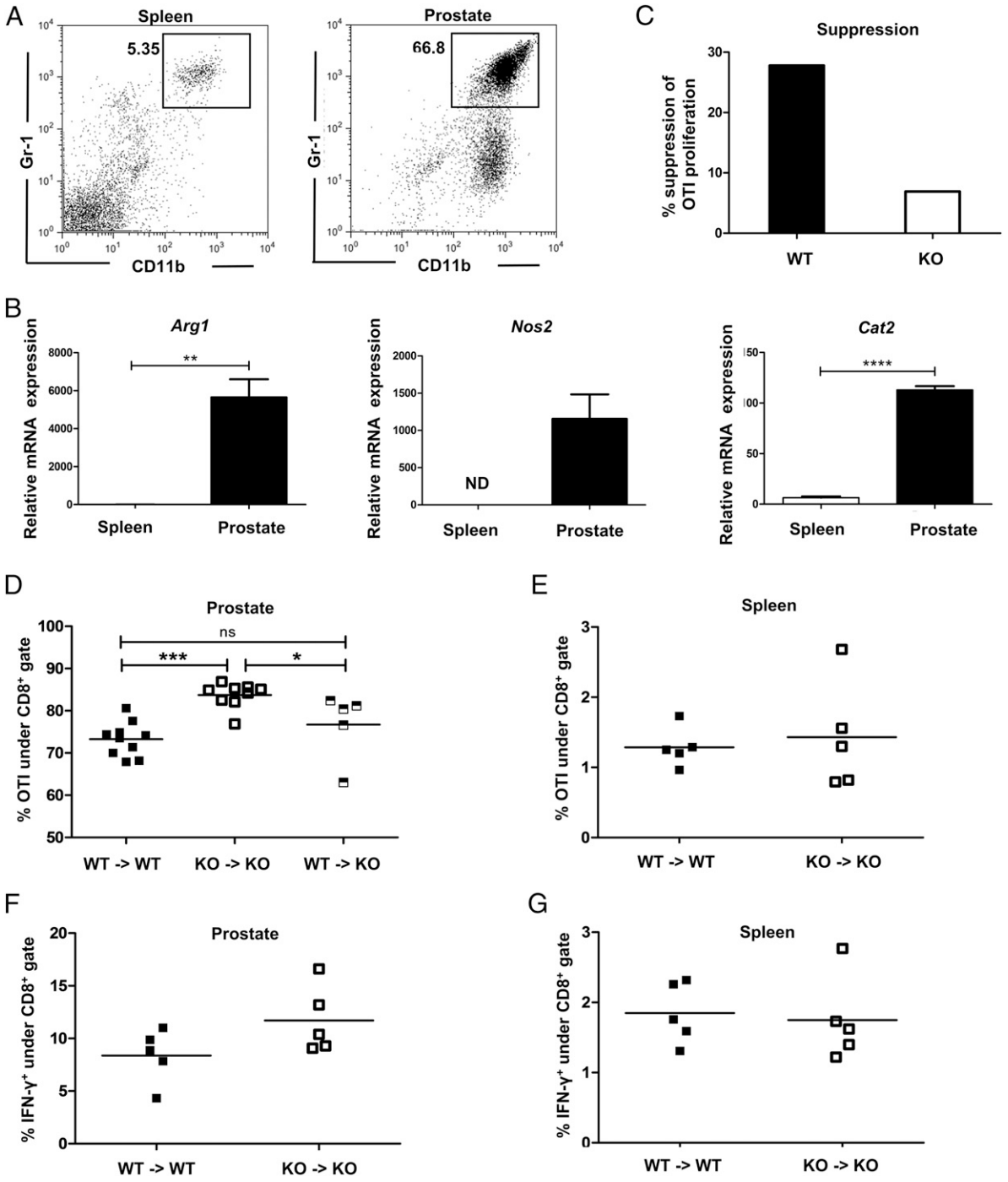

FIGURE 8. CAT2 modulates MDSC regulatory functions in an acute prostate inflammation model. POET-3 mice (n = 3) were injected with 5×10^6 activated OTI cells to induce prostate inflammation. Five days later, spleen and prostate $CD11b^+Gr\text{-}1^+$ cells (under $CD45^+$ gate) (**A**) were sorted by FACS. mRNA was freshly isolated from sorted cells and analyzed by qPCR for *Arg1*, *Nos2*, and *Cat2* expression (**B**). MDSCs were isolated from inflamed prostates of $Cat2^{+/+}$ and $Cat2^{-/-}$ POET-3 mice (n = 3/group, pooled) and cocultured with preactivated OTI cells for 48 h. BrdU was added 6 h before harvest. OTI proliferation was evaluated by measuring BrdU incorporation. Data are representative of at least three independent experiments (**$p = 0.038$, ****$p < 0.0001$). (**C**). A total of 5×10^6 activated OTI cells were i.v. injected into POET-3 mice to induce inflammation. Two days later, mice were adoptively transferred (i.p.) with 4×10^6 $Cat2^{+/+}$ and $Cat2^{-/-}$ bone marrow cells that were cultured 5 d with GM-CSF and IL-6. $Cat2^{+/+}$ POET-3 received $Cat2^{+/+}$ cells and $Cat2^{-/-}$ POET-3 received $Cat2^{-/-}$ or $Cat2^{+/+}$ cells. Percentage of $Thy1.1^+$ (OTI) cells in 5-d inflamed POET-3 prostate (**D**) and spleen (**E**) are represented under $CD45^+CD8^+$ gate. Each individual datum point represents a single mouse (***$p < 0.001$, *$p < 0.05$). Prostate (**F**) and spleen (**G**) cells were cultured with SIINFEKL and protein transport inhibitor for 8 h, and IFN-γ was detected by intracellular staining for flow cytometry. Data are representative for at least two independent experiments. Errors bars indicate ± SEM.

amino acids by MDSCs (34). For example, MDSCs express enzymes that metabolize L-Arg, L-tryptophan, and cysteine, leading to their consumption from the microenvironment. Depletion of these amino acids results in T cell dysfunction (35–37). In addition, MDSCs can metabolize L-Arg and L-phenylalanine, and generate end products that block T cell activities (38, 39). Among these, L-Arg metabolism is considered to be the hallmark mechanism for MDSC-mediated T cell inhibition (11). Therefore, in this study,

we focused on the mechanism and functional impact of L-Arg uptake on MDSCs. We postulated that we could control MDSC activity by modulating L-Arg entry into cells. L-Arg transport is mediated by y^+, y^+L and $b^{0,+}$, $B^{0,+}$ systems (13). The y^+ system member CAT2 was shown to be the dominant L-Arg transporter in macrophages and was indirectly implicated as a transporter in MDSCs (12). However, studies defining CAT2 as an L-Arg transporter and evaluation of the functional impact of CAT2 on MDSC function are lacking. Therefore, we initiated studies to define the role of CAT2 in MDSCs.

Our data demonstrate that *Cat2* expression is induced in $CD11b^+Gr\text{-}1^+$ cells only when they are exposed to activating cytokines in vitro. In vivo, only MDSCs that reside at inflammatory or tumor sites, but not at peripheral sites, have elevated *Cat2* expression. In addition, *Cat2* induction is coordinately expressed with *Nos2* and *Arg1*. Notably, the data reported in this study show that MDSC regulation of T cell immunity is compromised in the absence of CAT2, leading to inhibition of tumor growth. Thus, *Cat2* may be useful in defining the functional state of $CD11b^+Gr\text{-}1^+$ cells and serving as a target for regulating MDSC function.

Increased NOS2 and ARG1 activities are suggested to necessitate elevated L-Arg uptake in MDSCs (30). We hypothesized that transportation through CAT2 is responsible for elevated L-Arg uptake in MDSCs because its expression is coordinately induced with *Nos2* and *Arg1*. By comparing L-[^{3}H]-Arg incorporation in $Cat2^{+/+}$ and $Cat2^{-/-}$ MDSCs, we showed that unlike macrophages where CAT2 is responsible for 90% of L-Arg transport, CAT2 mediates only ~20% of L-Arg transport in MDSCs. These data suggested that other L-Arg transport mechanisms compensate for the loss of CAT2. Evaluation of the contribution of other known L-Arg transporters showed that no members of $b^{0,+}$ or $B^{0,+}$ were expressed in MDSCs. To further verify these results, we blocked the transport through $b^{0,+}$ or $B^{0,+}$ systems in MDSCs and did not observe any alterations in L-Arg uptake (data not shown). These results are similar to Martín et al.'s findings that $b^{0,+}$ or $B^{0,+}$ systems do not contribute to L-Arg transport in bone marrow–derived macrophages (17). We also investigated the participation of y^+L system in L-Arg transport in MDSCs and found that transport through the y^+L system accounts for ~25% of total transport. It is reported that in bone marrow cells, in addition to carrier-mediated transport through y^+ and y^+L systems, L-Arg can be taken up into cells by basal diffusion (17, 40). Indeed, we observed that a component of L-Arg uptake in MDSCs could not be blocked by addition of saturating levels of nonradioactive L-Arg in transportation assays (data not shown). Therefore, it is likely that in MDSCs, basal diffusion or an unidentified L-Arg carrier is responsible for the y^+- and y^+L-independent L-Arg transport. In addition, we observed that L-Arg uptake was ~10-fold higher in activated macrophages compared with MDSCs. Comparative qPCR analysis revealed that macrophages had higher *Cat2* expression than MDSCs (data not shown). Although this observation might explain why macrophages have higher L-Arg uptake than MDSCs, it is previously reported that mRNA levels of CATs do not necessarily reflect protein levels (14). Therefore, it is possible that the increase in *Cat2* gene expression in MDSCs may not correlate with the functional protein levels. Unfortunately, because of lack of availability of specific Abs we could not monitor CAT2 protein levels. Despite the compelling differences in L-Arg uptake through CAT2, NO production between MDSCs and macrophages was altered in an equivalent manner in the absence of CAT2 (~70% for each cell type). One possible explanation for these observations is that L-Arg compartmentalization might vary between the two cell types. It is proposed that there are distinct L-Arg pools inside the cells, and the access of NOS2 to distinct pools might differ between different cell types (14, 41).

Importantly, our data revealed that CAT2 expression in MDSCs regulates suppressive function. In the absence of CAT2, MDSCs have lower suppressive activity because of lower production of NO. Because NOS2 expression is not modulated by CAT2, reduced NO levels in $Cat2^{-/-}$ MDSCs is likely to be related to lower substrate availability. Similar to NOS2, ARG1 expression is also independent of CAT2 and in an arginase functional assay, $Cat2^{+/+}$ and $Cat2^{-/-}$ MDSCs displayed comparable arginase activity. This observation differs from a previous report that shows CAT2 deficiency enhances the activity of arginase in alternatively activated macrophages (24). Given the differences reported in this study between MDSCs and macrophages regarding CAT2 expression and CAT2-mediated L-Arg transport, it is possible that CAT2-dependent modulation of ARG1 activity also varies between the two cell types. Also, it is important to stress that unlike in the Griess reaction, in this urea detection assay we lyse the MDSCs and supply extracellular L-Arg for ARG1 enzyme to use. Hence this assay measures the capacity of the enzyme to catalyze L-Arg, but it does not reflect the intracellular activity of ARG1 in intact MDSCs in the absence or presence of CAT2. We anticipate that in $Cat2^{-/-}$ MDSCs, like NOS2, ARG1 activity is also reduced because CAT2 mediates its effects by controlling the substrate availability.

To further characterize CAT2-mediated MDSC suppressive function, we investigated the role of previously described MDSC suppressive mechanisms. Inhibitor studies suggested that in the RM1 ascites model, MDSC activity is mainly mediated through NOS2 activity. NOS inhibitor L-NMMA completely abrogated the suppressive function in MDSCs even at high MDSC/OTI ratios, whereas the arginase inhibitor, nor-NOHA, had no effect. This observation might be linked to the suppression assay used, where MDSCs and OTIs are engaged in cell–cell contact to monitor Ag-specific stimulation of OTI. Unlike NOS2, ARG1-mediated MDSC suppressive mechanisms have been reported to be independent of cell–cell contact (12, 42). In support of these results, Raber et al. (10) also showed that in a suppression assay, where MDSCs are in direct contact with T cells, L-NMMA completely blocked MDSC suppressive effect, whereas nor-NOHA had no effect. Although L-NMMA further inhibited the already reduced suppressive effect of $Cat2^{-/-}$ MDSCs, we still detected residual suppressive activity, unlike $Cat2^{+/+}$ MDSCs. It was reported previously that L-NMMA is transported through the y^+ system and has the same affinity for transporters as L-Arg (43). Therefore, it is likely that L-NMMA uptake in CAT2 ablated MDSCs is lower and may be insufficient to completely block suppressive activity. Alternatively, this result may suggest that $Cat2^{-/-}$ MDSCs uses NO-independent mechanisms to mediate T cell suppression. Because NOS2 in L-Arg–depleted macrophages produce $\cdot O_2^-$ rather than the common product NO (25) and ROS formation is a suppressive mechanism of MDSCs (26, 44), we evaluated ROS formation in MDSCs. Indeed, we detected elevated levels of ROS in $Cat2^{-/-}$ MDSCs. Inhibition of ROS resulted in greater changes in suppressive activity of $Cat2^{-/-}$ MDSCs than $Cat2^{+/+}$ MDSCs. ROS could mediate suppressive activity of WT MDSCs only at low MDSC/OTI ratios. Overall, our data indicate that reduced suppressive capacity of $Cat2^{-/-}$ MDSCs is due to lower NO production. $Cat2^{-/-}$ MDSCs depend more on ROS to suppress T cells than $Cat2^{+/+}$ MDSCs, and ROS-mediated suppression, at least in part, accounts for the residual suppression in $Cat2^{-/-}$ MDSCs. More studies are needed to investigate other CAT2-related suppressive mechanisms.

We also demonstrated that CAT2 is an important mediator of MDSC regulatory functions using in vivo models of acute inflammation and tumor formation. In the prostate-specific inflammation model (POET-3), in the absence of CAT2, adoptively transferred OTI cells displayed enhanced expansion and higher frequency of IFN-γ–producing cells in the prostate. No differences were observed in splenic OTI cells, which is consistent with their activation state. These results are in accordance with our previous findings that showed when MDSC function is blocked by anti–Gr-1 during acute prostate inflammation, OTI proliferation, and function is enhanced in the prostate, but not in the spleen (22). By controlling T cell function, MDSCs promote tumor progression, so ablation of CAT2 in MDSCs is expected to slow down tumor growth. To determine the effects of CAT2-mediated MDSC suppressive activity on tumor growth, we adopted an EG7 immunotherapy model (27). We implanted EG7 cells into $Cat2^{+/+}$ and $Cat2^{-/-}$ mice intradermally or s.c., and after 7 d we injected activated OTI cells i.v. In $Cat2^{-/-}$ mice, tumor growth was slower compared with $Cat2^{+/+}$ mice. These observations, together with results from the Winn assay, indicate that $Cat2^{-/-}$ MDSCs have diminished capacity to control antitumor T cell responses. However, it is important to mention that, in the absence of OTI transfer, EG7 growth was not significantly different between $Cat2^{+/+}$ and $Cat2^{-/-}$ mice. In fact, tumor growth rate was comparable also in EL4, MB49, and RM1 tumor models (data not shown). CAT2 is an important regulator for other cell types as well, including macrophages and T cells (45, 46). The reason that tumor growth in $Cat2^{-/-}$ mice is not slower is most likely because of the CAT2-related deficiencies in other cell types, especially T cells. *Cat2* is expressed in activated T cells (46, 47), and L-Arg is essential for T cell functions (48, 49). Further studies are needed to elucidate the CAT2-dependent regulatory functions of multiple populations present in the tumor microenvironment.

Together, our findings describe the contribution of different L-Arg transportation systems in MDSCs and define CAT2 as a major transporter that is induced in MDSCs with immediate suppressor function. Therefore, CAT2 is a marker for functionally active MDSCs. In addition, we demonstrate that CAT2 is a novel molecule mediating MDSC suppressive function and causing diminished antitumor immune responses. Hence CAT2 may be used as a target to modulate MDSC activity in inflammatory diseases.

Acknowledgments

We thank Drs. Jeff Woodliff and Jill Hutchcroft at Purdue Flow Cytometry and Cell Separation Facility for cell sorting.

Disclosures

The authors have no financial conflicts of interest.

References

1. Gabrilovich, D. I., and S. Nagaraj. 2009. Myeloid-derived suppressor cells as regulators of the immune system. *Nat. Rev. Immunol.* 9: 162–174.
2. Casbon, A.-J., D. Reynaud, C. Park, E. Khuc, D. D. Gan, K. Schepers, E. Passegué, and Z. Werb. 2015. Invasive breast cancer reprograms early myeloid differentiation in the bone marrow to generate immunosuppressive neutrophils. *Proc. Natl. Acad. Sci. USA* 112: E566–E575.
3. Walter, S., T. Weinschenk, A. Stenzl, R. Zdrojowy, A. Pluzanska, C. Szczylik, M. Staehler, W. Brugger, P.-Y. Dietrich, R. Mendrzyk, et al. 2012. Multipeptide immune response to cancer vaccine IMA901 after single-dose cyclophosphamide associates with longer patient survival. *Nat. Med.* 18: 1254–1261.
4. Gabitass, R. F., N. E. Annels, D. D. Stocken, H. A. Pandha, and G. W. Middleton. 2011. Elevated myeloid-derived suppressor cells in pancreatic, esophageal and gastric cancer are an independent prognostic factor and are associated with significant elevation of the Th2 cytokine interleukin-13. *Cancer Immunol. Immunother.* 60: 1419–1430.
5. Wesolowski, R., J. Markowitz, and W. E. Carson, III. 2013. Myeloid derived suppressor cells - a new therapeutic target in the treatment of cancer. *J. Immunother. Cancer* 1: 10.
6. Haile, L. A., R. von Wasielewski, J. Gamrekelashvili, C. Krüger, O. Bachmann, A. M. Westendorf, J. Buer, R. Liblau, M. P. Manns, F. Korangy, and T. F. Greten. 2008. Myeloid-derived suppressor cells in inflammatory bowel disease: a new immunoregulatory pathway. *Gastroenterology* 135: 871–881, 881.e1–5.
7. Zhu, B., Y. Bando, S. Xiao, K. Yang, A. C. Anderson, V. K. Kuchroo, and S. J. Khoury. 2007. CD11b+Ly-6C(hi) suppressive monocytes in experimental autoimmune encephalomyelitis. *J. Immunol.* 179: 5228–5237.
8. Fujii, W., E. Ashihara, H. Hirai, H. Nagahara, N. Kajitani, K. Fujioka, K. Murakami, T. Seno, A. Yamamoto, H. Ishino, et al. 2013. Myeloid-derived suppressor cells play crucial roles in the regulation of mouse collagen-induced arthritis. *J. Immunol.* 191: 1073–1081.
9. Haverkamp, J. M., A. M. Smith, R. Weinlich, C. P. Dillon, J. E. Qualls, G. Neale, B. Koss, Y. Kim, V. Bronte, M. J. Herold, et al. 2014. Myeloid-derived suppressor activity is mediated by monocytic lineages maintained by continuous inhibition of extrinsic and intrinsic death pathways. *Immunity* 41: 947–959.
10. Raber, P. L., P. Thevenot, R. Sierra, D. Wyczechowska, D. Halle, M. E. Ramirez, A. C. Ochoa, M. Fletcher, C. Velasco, A. Wilk, et al. 2014. Subpopulations of myeloid-derived suppressor cells impair T cell responses through independent nitric oxide-related pathways. *Int. J. Cancer* 134: 2853–2864.
11. Bronte, V., and P. Zanovello. 2005. Regulation of immune responses by L-arginine metabolism. *Nat. Rev. Immunol.* 5: 641–654.
12. Raber, P., A. C. Ochoa, and P. C. Rodríguez. 2012. Metabolism of L-arginine by myeloid-derived suppressor cells in cancer: mechanisms of T cell suppression and therapeutic perspectives. *Immunol. Invest.* 41: 614–634.
13. Devés, R., and C. A. Boyd. 1998. Transporters for cationic amino acids in animal cells: discovery, structure, and function. *Physiol. Rev.* 78: 487–545.
14. Closs, E. I., A. Simon, N. Vékony, and A. Rotmann. 2004. Plasma membrane transporters for arginine. *J. Nutr.* 134: 2752S–2759S; discussion 2765S–2767S.
15. Verrey, F., E. I. Closs, C. A. Wagner, M. Palacin, H. Endou, and Y. Kanai. 2004. CATs and HATs: the SLC7 family of amino acid transporters. *Pflugers Arch.* 447: 532–542.
16. Nicholson, B., C. K. Manner, J. Kleeman, and C. L. MacLeod. 2001. Sustained nitric oxide production in macrophages requires the arginine transporter CAT2. *J. Biol. Chem.* 276: 15881–15885.
17. Martín, L., M. Comalada, L. Marti, E. I. Closs, C. L. MacLeod, R. Martín del Río, A. Zorzano, M. Modolell, A. Celada, M. Palacín, and J. Bertran. 2006. Granulocyte-macrophage colony-stimulating factor increases L-arginine transport through the induction of CAT2 in bone marrow-derived macrophages. *Am. J. Physiol. Cell Physiol.* 290: C1364–C1372.
18. Rodriguez, P. C., D. G. Quiceno, J. Zabaleta, B. Ortiz, A. H. Zea, M. B. Piazuelo, A. Delgado, P. Correa, J. Brayer, E. M. Sotomayor, et al. 2004. Arginase I production in the tumor microenvironment by mature myeloid cells inhibits T-cell receptor expression and antigen-specific T-cell responses. *Cancer Res.* 64: 5839–5849.
19. Lees, J. R., B. Charbonneau, J. D. Hayball, K. Diener, M. Brown, R. Matusik, M. B. Cohen, and T. L. Ratliff. 2006. T-cell recognition of a prostate specific antigen is not sufficient to induce prostate tissue destruction. *Prostate* 66: 578–590.
20. Qualls, J. E., C. Subramanian, W. Rafi, A. M. Smith, L. Balouzian, A. A. DeFreitas, K. A. Shirey, B. Reutterer, E. Kernbauer, S. Stockinger, et al. 2012. Sustained generation of nitric oxide and control of mycobacterial infection requires argininosuccinate synthase 1. *Cell Host Microbe* 12: 313–323.
21. Gallina, G., L. Dolcetti, P. Serafini, C. De Santo, I. Marigo, M. P. Colombo, G. Basso, F. Brombacher, I. Borrello, P. Zanovello, et al. 2006. Tumors induce a subset of inflammatory monocytes with immunosuppressive activity on CD8+ T cells. *J. Clin. Invest.* 116: 2777–2790.
22. Haverkamp, J. M., S. A. Crist, B. D. Elzey, C. Cimen, and T. L. Ratliff. 2011. In vivo suppressive function of myeloid-derived suppressor cells is limited to the inflammatory site. *Eur. J. Immunol.* 41: 749–759.
23. Corzo, C. A., T. Condamine, L. Lu, M. J. Cotter, J.-I. Youn, P. Cheng, H.-I. Cho, E. Celis, D. G. Quiceno, T. Padhya, et al. 2010. HIF-1α regulates function and differentiation of myeloid-derived suppressor cells in the tumor microenvironment. *J. Exp. Med.* 207: 2439–2453.
24. Thompson, R. W., J. T. Pesce, T. Ramalingam, M. S. Wilson, S. White, A. W. Cheever, S. M. Ricklefs, S. F. Porcella, L. Li, L. G. Ellies, and T. A. Wynn. 2008. Cationic amino acid transporter-2 regulates immunity by modulating arginase activity. *PLoS Pathog.* 4: e1000023.
25. Xia, Y., and J. L. Zweier. 1997. Superoxide and peroxynitrite generation from inducible nitric oxide synthase in macrophages. *Proc. Natl. Acad. Sci. USA* 94: 6954–6958.
26. Corzo, C. A., M. J. Cotter, P. Cheng, F. Cheng, S. Kusmartsev, E. Sotomayor, T. Padhya, T. V. McCaffrey, J. C. McCaffrey, and D. I. Gabrilovich. 2009. Mechanism regulating reactive oxygen species in tumor-induced myeloid-derived suppressor cells. *J. Immunol.* 182: 5693–5701.
27. Helmich, B. K., and R. W. Dutton. 2001. The role of adoptively transferred CD8 T cells and host cells in the control of the EG7 thymoma: factors that determine the relative effectiveness and homing properties of Tc1 and Tc2 effectors. *J. Immunol.* 166: 6500–6508.
28. Haverkamp, J. M., B. Charbonneau, S. A. Crist, D. K. Meyerholz, M. B. Cohen, P. W. Snyder, R. U. Svensson, M. D. Henry, H.-H. Wang, and T. L. Ratliff. 2011. An inducible model of abacterial prostatitis induces antigen specific inflammatory and proliferative changes in the murine prostate. *Prostate* 71: 1139–1150.
29. Marigo, I., E. Bosio, S. Solito, C. Mesa, A. Fernandez, L. Dolcetti, S. Ugel, N. Sonda, S. Bicciato, E. Falisi, et al. 2010. Tumor-induced tolerance and im-

mune suppression depend on the C/EBPbeta transcription factor. *Immunity* 32: 790–802.
30. Ostrand-Rosenberg, S. 2010. Myeloid-derived suppressor cells: more mechanisms for inhibiting antitumor immunity. *Cancer Immunol. Immunother.* 59: 1593–1600.
31. Iclozan, C., S. Antonia, A. Chiappori, D.-T. Chen, and D. Gabrilovich. 2013. Therapeutic regulation of myeloid-derived suppressor cells and immune response to cancer vaccine in patients with extensive stage small cell lung cancer. *Cancer Immunol. Immunother.* 62: 909–918.
32. Highfill, S. L., Y. Cui, A. J. Giles, J. P. Smith, H. Zhang, E. Morse, R. N. Kaplan, and C. L. Mackall. 2014. Disruption of CXCR2-mediated MDSC tumor trafficking enhances anti-PD1 efficacy. *Sci. Transl. Med.* 6: 237ra67.
33. Ostrand-Rosenberg, S., and P. Sinha. 2009. Myeloid-derived suppressor cells: linking inflammation and cancer. *J. Immunol.* 182: 4499–4506.
34. Marigo, I., L. Dolcetti, P. Serafini, P. Zanovello, and V. Bronte. 2008. Tumor-induced tolerance and immune suppression by myeloid derived suppressor cells. *Immunol. Rev.* 222: 162–179.
35. Fallarino, F., U. Grohmann, S. You, B. C. McGrath, D. R. Cavener, C. Vacca, C. Orabona, R. Bianchi, M. L. Belladonna, C. Volpi, et al. 2006. The combined effects of tryptophan starvation and tryptophan catabolites down-regulate T cell receptor zeta-chain and induce a regulatory phenotype in naive T cells. *J. Immunol.* 176: 6752–6761.
36. Rodriguez, P. C., A. H. Zea, J. DeSalvo, K. S. Culotta, J. Zabaleta, D. G. Quiceno, J. B. Ochoa, and A. C. Ochoa. 2003. L-arginine consumption by macrophages modulates the expression of CD3 zeta chain in T lymphocytes. *J. Immunol.* 171: 1232–1239.
37. Srivastava, M. K., P. Sinha, V. K. Clements, P. Rodriguez, and S. Ostrand-Rosenberg. 2010. Myeloid-derived suppressor cells inhibit T-cell activation by depleting cystine and cysteine. *Cancer Res.* 70: 68–77.
38. Nagaraj, S., K. Gupta, V. Pisarev, L. Kinarsky, S. Sherman, L. Kang, D. L. Herber, J. Schneck, and D. I. Gabrilovich. 2007. Altered recognition of antigen is a mechanism of CD8+ T cell tolerance in cancer. *Nat. Med.* 13: 828–835.
39. Boulland, M. L., J. Marquet, V. Molinier-Frenkel, P. Möller, C. Guiter, F. Lasoudris, C. Copie-Bergman, M. Baia, P. Gaulard, K. Leroy, and F. Castellano. 2007. Human IL4I1 is a secreted L-phenylalanine oxidase expressed by mature dendritic cells that inhibits T-lymphocyte proliferation. *Blood* 110: 220–227.
40. Speake, P. F., J. D. Glazier, P. T. Y. Ayuk, M. Reade, C. P. Sibley, and S. W. D'Souza. 2003. L-Arginine transport across the basal plasma membrane of the syncytiotrophoblast of the human placenta from normal and preeclamptic pregnancies. *J. Clin. Endocrinol. Metab.* 88: 4287–4292.
41. Closs, E. I., J. S. Scheld, M. Sharafi, and U. Förstermann. 2000. Substrate supply for nitric-oxide synthase in macrophages and endothelial cells: role of cationic amino acid transporters. *Mol. Pharmacol.* 57: 68–74.
42. Rodríguez, P. C., and A. C. Ochoa. 2008. Arginine regulation by myeloid derived suppressor cells and tolerance in cancer: mechanisms and therapeutic perspectives. *Immunol. Rev.* 222: 180–191.
43. Schmidt, K., P. Klatt, and B. Mayer. 1993. Characterization of endothelial cell amino acid transport systems involved in the actions of nitric oxide synthase inhibitors. *Mol. Pharmacol.* 44: 615–621.
44. Kusmartsev, S., Y. Nefedova, D. Yoder, and D. I. Gabrilovich. 2004. Antigen-specific inhibition of CD8+ T cell response by immature myeloid cells in cancer is mediated by reactive oxygen species. *J. Immunol.* 172: 989–999.
45. Ezernitchi, A. V., I. Vaknin, L. Cohen-Daniel, O. Levy, E. Manaster, A. Halabi, E. Pikarsky, L. Shapira, and M. Baniyash. 2006. TCR zeta down-regulation under chronic inflammation is mediated by myeloid suppressor cells differentially distributed between various lymphatic organs. *J. Immunol.* 177: 4763–4772.
46. MacLeod, C. L., K. Finley, D. Kakuda, C. A. Kozak, and M. F. Wilkinson. 1990. Activated T cells express a novel gene on chromosome 8 that is closely related to the murine ecotropic retroviral receptor. *Mol. Cell. Biol.* 10: 3663–3674.
47. Reizer, J., K. Finley, D. Kakuda, C. L. MacLeod, A. Reizer, and M. H. Saier, Jr. 1993. Mammalian integral membrane receptors are homologous to facilitators and antiporters of yeast, fungi, and eubacteria. *Protein Sci.* 2: 20–30.
48. Rodriguez, P. C., D. G. Quiceno, and A. C. Ochoa. 2007. L-arginine availability regulates T-lymphocyte cell-cycle progression. *Blood* 109: 1568–1573.
49. Zea, A. H., P. C. Rodriguez, K. S. Culotta, C. P. Hernandez, J. DeSalvo, J. B. Ochoa, H.-J. Park, J. Zabaleta, and A. C. Ochoa. 2004. L-Arginine modulates CD3zeta expression and T cell function in activated human T lymphocytes. *Cell. Immunol.* 232: 21–31.

Supplemental Figure 1

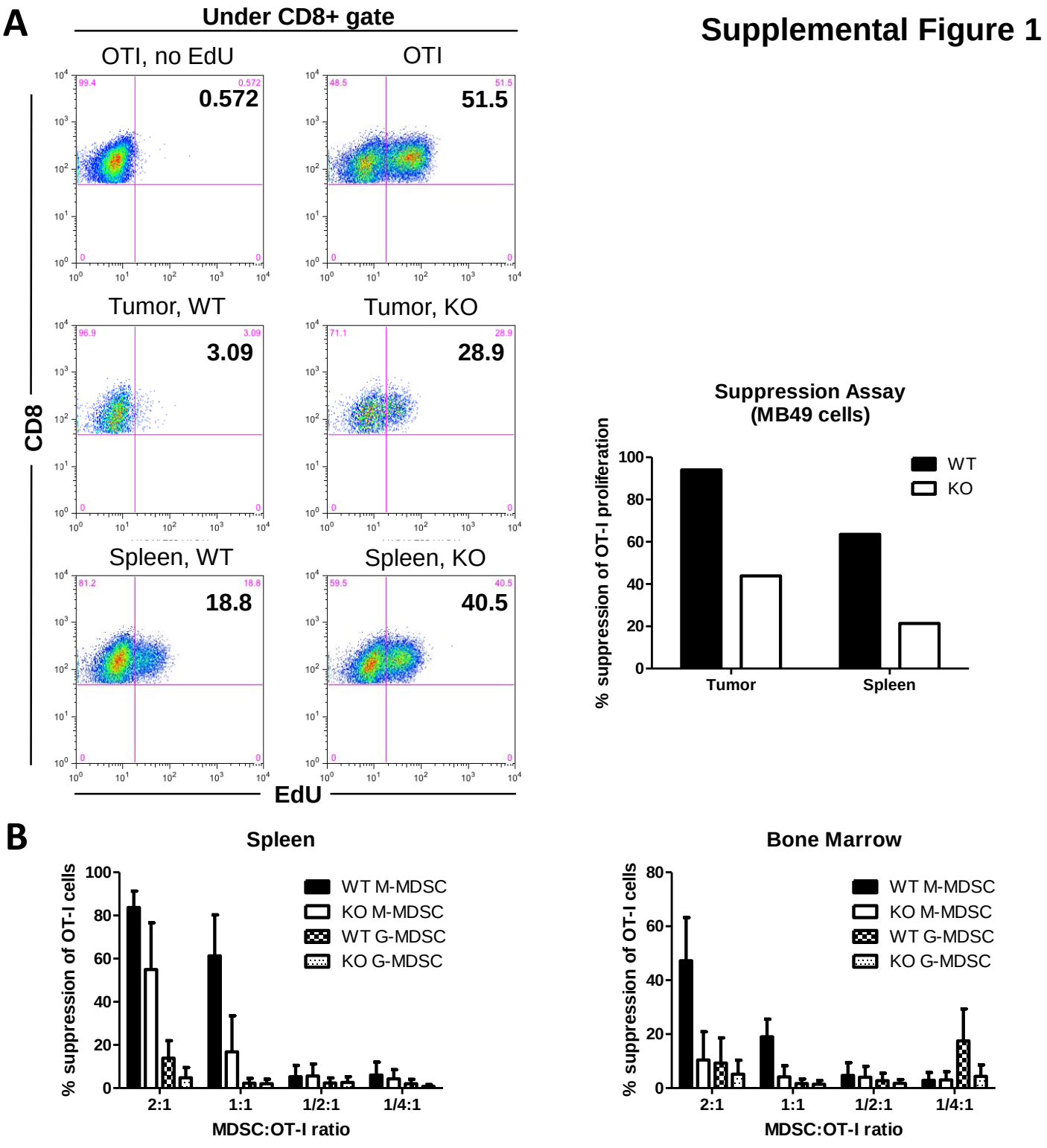

CAT2 regulates MDSC suppressive capacity. (A) *Cat2*$^{+/+}$ (WT) and *Cat2*$^{-/-}$ (KO) mice were subcutaneously injected with 5x10^5 MB49 bladder cancer cells (n=7 mice/group, pooled). CD11b$^+$Gr-1$^+$ cells were isolated by FACS from the tumor site and spleen and co-cultured with preactivated OTI cells at 1:1 ratio for 48 hours. EdU was added 2 hours before harvest. OTI proliferation was evaluated by measuring EdU incorporation. Data are representative of 2 independent experiments**. (B)** M-MDSC and G-MDSC were isolated by FACS from the spleens and bone marrow of RM1 i.p. tumor bearing WT and KO mice (n=3-5/group, pooled) 6 days after tumor implantation and co-cultured with naive OTI cells with SIINFEKL for 48-72 hours. BrdU added 6 hours before harvest. OTI proliferation was evaluated by measuring BrdU incorporation. Data are pooled from 4 independent experiments. Errors bars indicate ±SEM.

Supplemental Figure 2

y^+ System

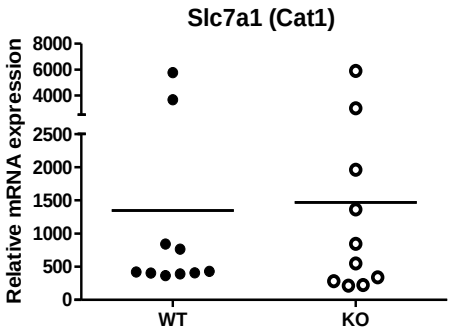

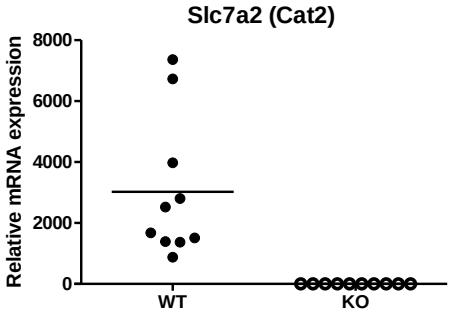

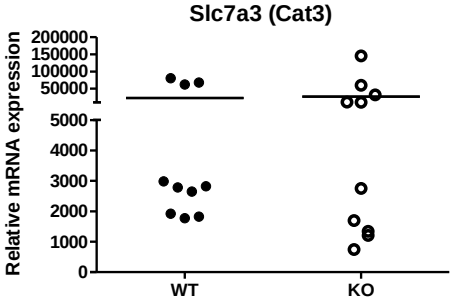

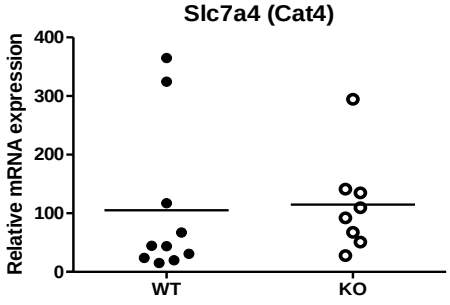

y^+L System

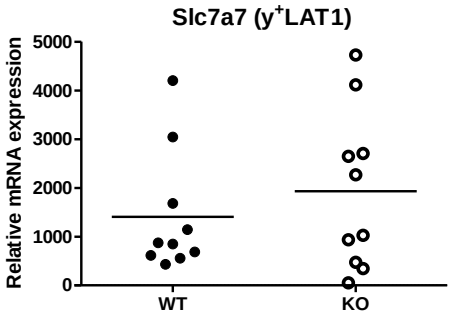

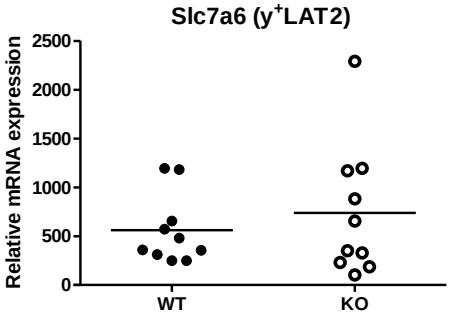

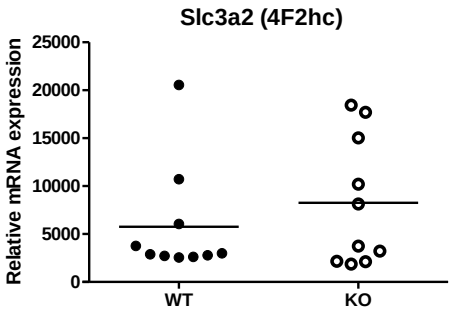

$b^{0,+}$ System

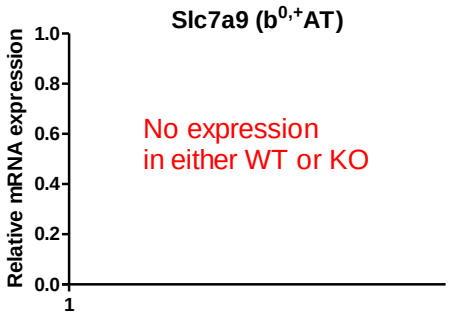

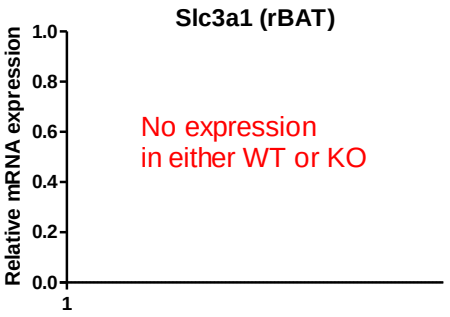

$B^{0,+}$ System

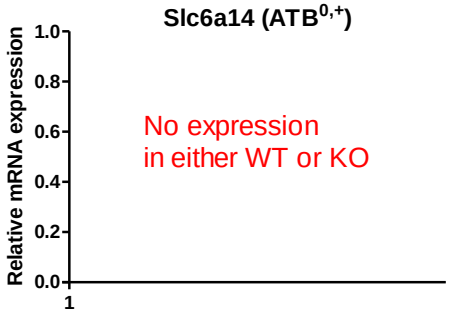

Expression of multiple transport systems in MDSC. $CD11b^+Gr\text{-}1^+$ cells were isolated by FACS from ascites of RM1 i.p. tumor bearing *Cat2*$^{+/+}$ (WT) and *Cat2*$^{-/-}$ (KO) mice and mRNA was freshly isolated and analyzed by qPCR for expression of L-Arg carriers that are members of y^+,y^+L, $b^{0,+}$, $B^{0,+}$ systems. Data are pooled from 3 independent experiments. Each data point indicates the expression level in an individual mouse.

Supplemental Figure 3

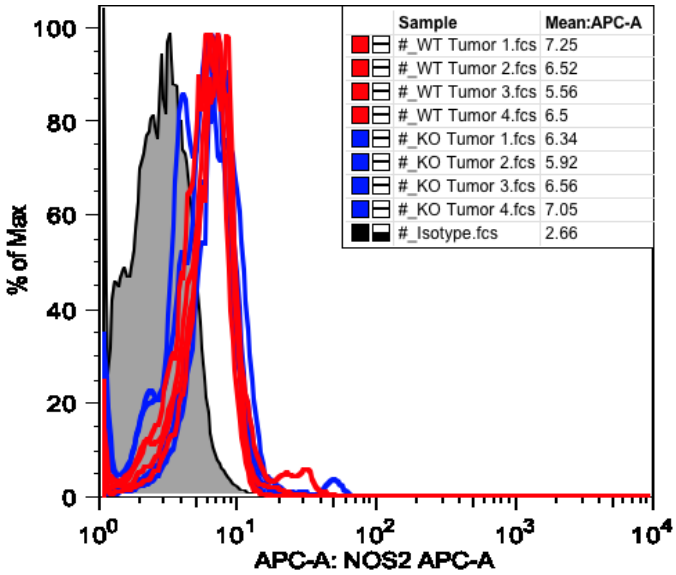

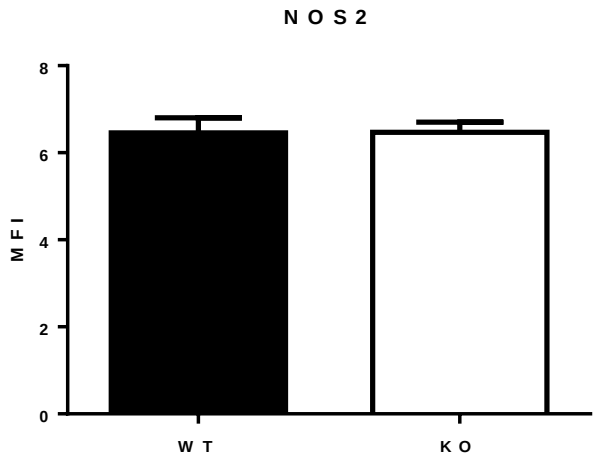

NOS2 protein expression in MDSC is independent of CAT2. Cells freshly isolated from the ascites of $CAT2^{+/+}$ and $CAT2^{-/-}$ RM1 mice were stained with anti-NOS2 antibody. NOS2 expression was detected by flow cytometry. Mean fluorescent intensity (MFI) of NOS2 expression was reported under $CD11b^{+}Gr\text{-}1^{+}$ gate (n=4/group). Data are representative of 4 independently performed experiments.

Supplemental Figure 4

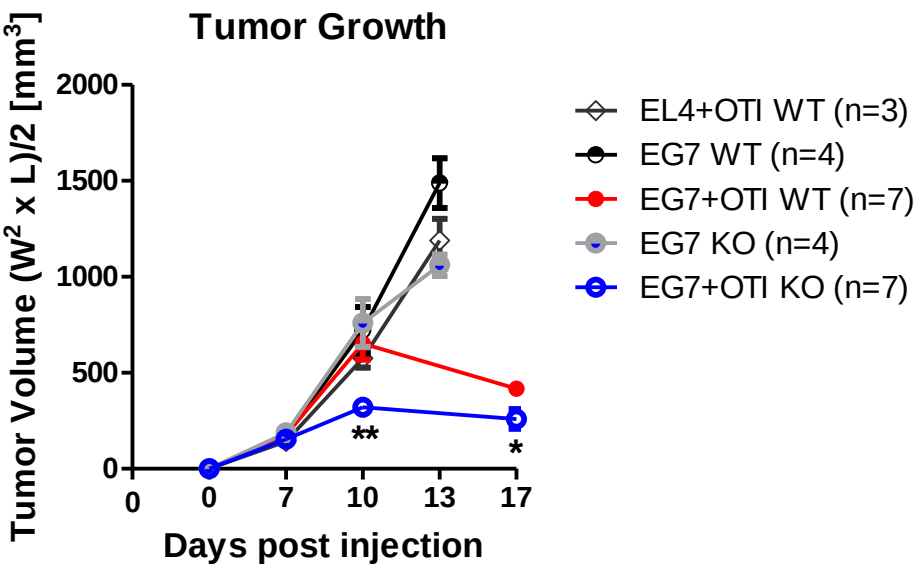

CAT2$^{-/-}$ MDSC display diminished capacity for controlling T-cell immunity *in vivo*. *Cat2*$^{+/+}$ and *Cat2*$^{-/-}$ mice were injected subcutaneously with 3x10^6 EG7 or EL4 lymphoma cells. 7 days after tumor inoculation, mice were intravenously injected with 10^6 activated OTI cells. Tumor growth was monitored. Tumor size was calculated as (W^2 x L) /2 [mm^3]. Errors bars indicate ±SEM. p values for the comparison of *Cat2*$^{+/+}$ and *Cat2*$^{-/-}$ mice that received OTI are 0.0023 and 0.0153 on Day 10 and 17, respectively. Data is representative of at least 2 independent experiments.